Iranian Journal of Science and Technology, Transactions of Civil Engineering (2021) 45:2733–2763
https://doi.org/10.1007/s40996-020-00540-4

RESEARCH PAPER

Modified Pseudo-dynamic Bearing Capacity of Strip Footing Resting on Layered Soil

Litan Debnath[1] · **Sima Ghosh**[1]

Received: 5 March 2020 / Accepted: 7 November 2020 / Published online: 5 January 2021

Abstract

Seismic bearing capacity analysis is an important aspect for the design of foundation in earthquake-prone areas. In this study, an attempt is made to evaluate the seismic bearing capacity of foundation resting on two-layered $c-\phi$ soil using a new pseudo-dynamic limit equilibrium approach considering linear failure surface and the soil supporting as a visco-elastic material. The results are expressed in terms of bearing capacity ratio. A comparison of the present method with other available literatures is presented, which shows the acceptability of the results of the present study. Hence, the results of the present study may be used to design seismically stable shallow strip footing.

Keywords Pseudo-static · Particle swarm optimization · Layered soil · Bearing capacity ratio · $c-\phi$ soil · Convergence

List of Symbols

B_0	Width of the footing
D_f	Depth of the footing
P_1	Combined load of column and footing
ξ_1	Damping ratio in top soil layer
ξ_2	Damping ratio in bottom soil layer
H	Total thickness of homogeneous soil layer
h_2	The thickness of the second layer contributing the failure wedge
h_1	The thickness of the top layer contributing the failure wedge
$N_{\gamma''}$	Single bearing capacity coefficient for coincident resistance of unit weight surcharge and cohesion
q_{ult}	Ultimate bearing capacity
G	Shear modulus of soil
η	Viscosity of soil
ξ	Damping ratio of homogeneous soil
G^*	Complex shear modulus of soil
k^*	Complex wave number
ρ_1	Density of top soil layer
ρ_2	Density of bottom soil layer
a_i	Acceleration amplitude of incident wave
a_r	Acceleration amplitude of reflected wave
a_t	Acceleration amplitude of transmitted wave
α_z	Impedance ratio
$(\alpha_z)_s$	Impedance ratio of shear wave
$(\alpha_z)_p$	Impedance ratio of primary wave
$y_{s1}, y_{s2}, y_{s5}, y_{s6}$	A dimensional factors governing horizontal acceleration at top soil layer due to transmitted wave
$y_{s3}, y_{s4}, y_{s7}, y_{s8}$	A dimensional factors governing horizontal acceleration at bottom soil layer due to incident and reflected waves
$Q_{t_{h(ABDE)}}$	Horizontal inertia force of the soil wedge ABDE due to transmitted wave
g	Acceleration due to gravity
A_{h_1}, B_{h_1}	Dimensionless numerical coefficient for horizontal inertia force at soil wedge ABDE
A_{h_2}, B_{h_2}	Dimensionless numerical coefficient for horizontal inertia force at soil wedge EDF
A_{h_3}, B_{h_3}	Dimensionless numerical coefficient for horizontal inertia force at soil wedge BJKD
A_{h_4}, B_{h_4}	Dimensionless numerical coefficient for horizontal inertia force at soil wedge DKF
v_{s1}	Shear wave velocity on top soil layer
v_{p1}	Primary wave velocity on top soil layer

✉ Litan Debnath
litandbnth4@gmail.com

Sima Ghosh
sima.civil@nita.ac.in

[1] Civil Engineering Department, National Institute of Technology, Agartala 799046, India

$Q_{i_{h(EDF)}}$	Horizontal inertia force of the soil wedge EDF due to incident wave
$m(z_2)_{(EDF)}$	Mass of soil wedge EDF
$a_{t_h(ABDE)}(z_1, t)$	Acceleration in horizontal direction due to transmitted wave in ABDE zone at depth z_1
$a_{t_{h_1}0}$	Acceleration amplitude in horizontal direction
$a_{t_{v(ABDE)}}(z_1, t)$	Acceleration in vertical direction due to transmitted wave
$a_{t_{v_1}0}$	Acceleration amplitude in vertical direction
$a_{i_{h(EDF)}}(z_2, t)$	Horizontal acceleration of incident wave on soil mass EDF at depth z_2 and time t
$a_{i_{h_2}0_{(EDF)}}$	Amplitude of horizontal acceleration of incident wave on soil mass EDF
$Q_{r_{h(EDF)}}$	Horizontal inertia force of the soil wedge EDF due to the reflected wave
$a_{r_{h(EDF)}}(z_2, t)$	Horizontal acceleration of reflected wave on soil mass EDF at depth z_2 and time t
$a_{r_{h_2}0_{(EDF)}}$	Amplitude of horizontal acceleration of reflected wave on soil mass EDF
$(Q_{h_{(EDF)}})_R$	Resultant horizontal inertia force of the soil wedge EDF
v_{s2}	Shear wave velocity on bottom soil layer
v_{p2}	Primary wave velocity on bottom soil layer
$Q_{t_{h(BJKD)}}$	Horizontal inertia force of the soil wedge BJKD due to transmitted wave
$Q_{i_{h(EDF)}}$	Horizontal inertia force of the soil wedge EDF due to incident wave

1 Introduction

Evaluation of seismic bearing capacity is an integral part of foundation design in the seismically active region. Several researchers have investigated bearing capacity of shallow strip footing using analytical, numerical and experimental methods. Numerous researchers have been analyzing the bearing capacity of shallow strip footing considering the underground soil as single layer of homogeneous soil. However, in nature soil is non-homogeneous and in some cases, different layers overlay to each other.

A innumerable number of researchers investigated the bearing capacity of shallow foundation on layered soil considering static loading condition (Button 1953; Reddy and Srinivasan 1967; Hanna and Meyerhof 1979; Florkiewicz 1989; Michalowski and Shi 1995; Michalowski 2002; Wang and Carter 2002; Kumar et al. 2007; Ghazavi and Eghbali 2008; Benmebarek et al. 2012; Karamitros et al. 2013; Ahmadi and Kouchaki 2016; Haghbin 2016; Khatri et al. 2017; Bera and Sasmal 2017; Biswas and Ghosh 2017; Mosallanezhad and Moayedi 2017; Jahani et al. 2018; Rajaei et al. 2018). To solve this problem, different failure surfaces such as linear, log-spiral are considered in the analysis. A comparison as given in Table 1 shows that there is no such difference in result.

Drominex and Pecker (1995), Soubra (1997) have developed the seismic bearing capacity factors for strip footings using upper-bound limit analysis. Many researchers have analyzed the seismic bearing capacity using the limit equilibrium method (Richards et al. 1993; Budhu and Al-Karni 1993; Saran and Agarwal 1991; Choudhury and Subba Rao 2006; Ghosh and Debnath 2017; Debnath and Ghosh 2018). In all the mentioned seismic analyses, the researchers have considered pseudo-static inertia forces, which are very crude approximation of earthquake dynamic forces where the time and phase lag are not considered. Jadar and Ghosh (2017), Saha and Ghosh (2015, 2019) have considered simultaneous resistance of unit weight, surcharge and cohesion to evaluate the bearing capacity of shallow strip footing. As an improvement of pseudo-static method, Steedman and Zeng (1990) have proposed a simple pseudo-dynamic method to analyze a vertical retaining wall in which only horizontal inertia force is considered. The proposed method is extensively used by numerous researchers (Choudhury and Nimbalkar 2005; Ghosh 2008; Saha and Ghosh 2015). However, pseudo-dynamic method lacks in certain aspects. For example, pseudo-dynamic method does not satisfy the boundary condition. It considers only incidental waves traveling upward through a linear elastic soil surface, resulting in a violation of the free-surface boundary condition. Pseudo-dynamic method follows a simple approach to consider the acceleration amplification. Linear variation of the acceleration is considered in this analysis. Also, the pseudo-dynamic method does not consider the damping properties of the soil. Whereas Bellezza (2014) has proposed a new pseudo-dynamic approach that considers the boundary condition, Pain et al. (2015) have showed that the wall–soil interaction in various seismic conditions may or may not be in phase for maximum sliding of the wall under active mode of failure. The researchers assumed a planar rupture surface. Pain et al. (2017) have applied this method to compute the passive earth pressure to take into account the negative wall friction angle under seismic loading conditions. Bellezza (2015) has taken into account the effect of both horizontal and vertical seismic accelerations to estimate the seismic active thrust assuming the soil as a Kelvin–Voigt solid. So, it is seen that new pseudo-dynamic method has advantages over pseudo-static and pseudo-dynamic, which is yet to be applied to solve foundation-related problems resting on two-layered soil.

Table 1 Comparison of ultimate bearing capacity between linear and log-spiral failure surfaces $\gamma = 18$ kN/m^3, $q = 18$ kN/m^2, $c = 15$ kN/m^2, $B_0 = 2.5$ m

Static ultimate bearing capacity (q_{ult}) kN/m^2							
Single-layer soil				Two-layered soil			
Linear	Values	Log-spiral	Values	Linear	Values	Log-spiral	Values
Richards et al. (1993)	1234.68	Terzaghi (1943)	1406.25	Ghazavi and Eghbali (2008)	1333	Purush-othamaraj et al. (1974)	1316.28
Ghosh and Debnath (2017)	1571.985	Meyerhof (1951)	1136.4	Debnath and Ghosh (2018)	1199	Hanna (1982)	1170
Soubra (1994)	1675.2	Hansen (1970)	1122.9				
Bowles(1996)	783.3	Griffiths (1982)	973.95				
Sokolovski (1965)	1126.95	Vesic (1973)	1287.15				
Saran (1971)	1622.25	Saran and Agarwal (1991)	1624.5				
		Prakash and Saran (1971)	1388.7				
		Soubra (1997)	1345.2				
		Soubra (1999)	1278.33				
		Saran et al. (1989)	1622.25				
		Choudhury and Subha Rao (2005)	1228.875				
		Eurocode7 (1996)	1235.175				

Hence, in the present study, an attempt is made to use this new pseudo-dynamic approach to evaluate the seismic bearing capacity of shallow strip footing resting on two-layered $c-\phi$ soil. Particle swarm optimization algorithm is used for optimization. Bearing capacity is evaluated as a single coefficient for the simultaneous action of unit weight, surcharge and cohesion, which is more practical to simulate the field situation.

2 Model Definition

A strip footing having a width of B_0 is assumed to be on the top of a two-layered $c-\phi$ soil as shown in Fig. 1. The water table is assumed to be well below the footing. The bearing capacity of a strip footing, q_{ult}, is normally computed using the following formulation

$$q_{ult} = \frac{1}{2}\gamma B_0 N_{\gamma''},$$

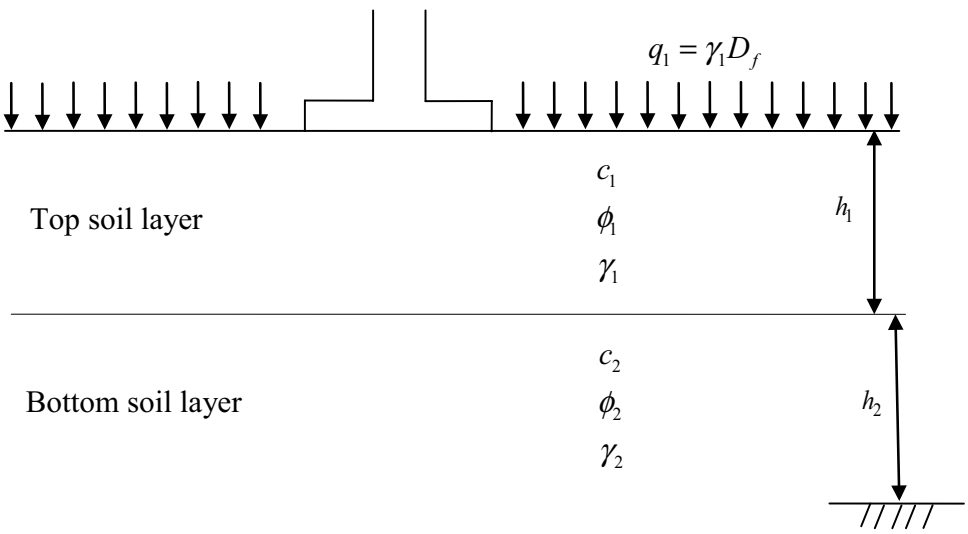

Fig. 1 Geometry of footing on two-layered

whereas $N_{\gamma''}$ is the single bearing capacity coefficient for simultaneous resistance of unit weight, surcharge and cohesion.

The failure surfaces are adopted as shown in Fig. 2. These were adopted by other investigators (Richards et al. 1993). As shown in Fig. 2, face BDF perpendicular to the base of the foundation is assumed to act like a retaining wall on which, at failure stage, active pressures resulting from q_{ult}, the weight of wedge ABDEF as soil pressure, are applied to the left side. On the right-hand side, surcharge $q_1 = \gamma_1 D_f$ and the weight of wedge BJKFD generate passive resistances on the vertical wall. At equilibrium, both these active pressure and passive resistances are equal.

3 Wave Propagation for Visco-Elastic Material

Consider P and S waves traveling along the visco-elastic soil layer in the upward direction and approaching an interface between two different soil layers as shown in Fig. 3. Since these waves traveling toward the interface, it will be referred to as an incident waves. When the incident waves reaches at the interface, the part of its energy will be transmitted through the interface to continue traveling in the upward direction through layer 1. The remainder will be reflected at the interface and will travel back through layer 2 in the downward direction as a reflected wave.

The reflected and refracted waves produced by incident P wave, S wave at interface are shown in Fig. 3. Table 2 shows the relation between amplitudes of different waves and angles formed by the waves with normal to the plane.

From Snell's Law, $\frac{\sin a}{X} = \frac{\sin b}{Y} = \frac{\sin c}{X} = \frac{\sin d}{Y} = \frac{\sin e}{Y} = \frac{\sin f}{Z}$ [For details-NPTEL-Geotechnical Earthquake Engineering, Module 2, Wave Propagation; Lecture 7–9].

The related terms in Snell's law are given in Table 2.

Assuming that the displacement associated with incident, reflected and transmitted waves are of same harmonic form and so writing down the corresponding displacement, acceleration and stress Eqs. acceleration amplitude is represented as:

$$\therefore a_r = \frac{1-\alpha_z}{1+\alpha_z} a_i \tag{1}$$

$$\therefore a_t = \frac{2}{1+\alpha_z} a_i \tag{2}$$

where

$$\alpha_z = \frac{\rho_1 v_1}{\rho_2 v_2}$$

Here, a_r = acceleration amplitude due to reflected wave a_i = acceleration amplitude due to incident wave a_t = acceleration amplitude due to transmitted wave

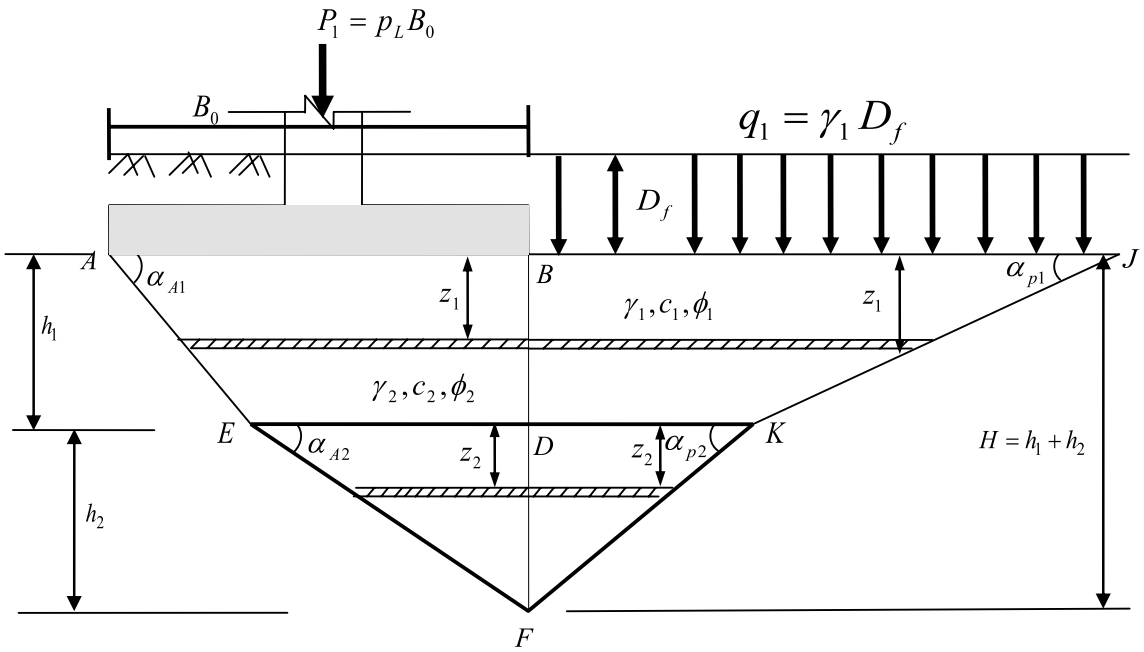

Fig. 2 Failure mechanism and wedges assumed in the present analysis

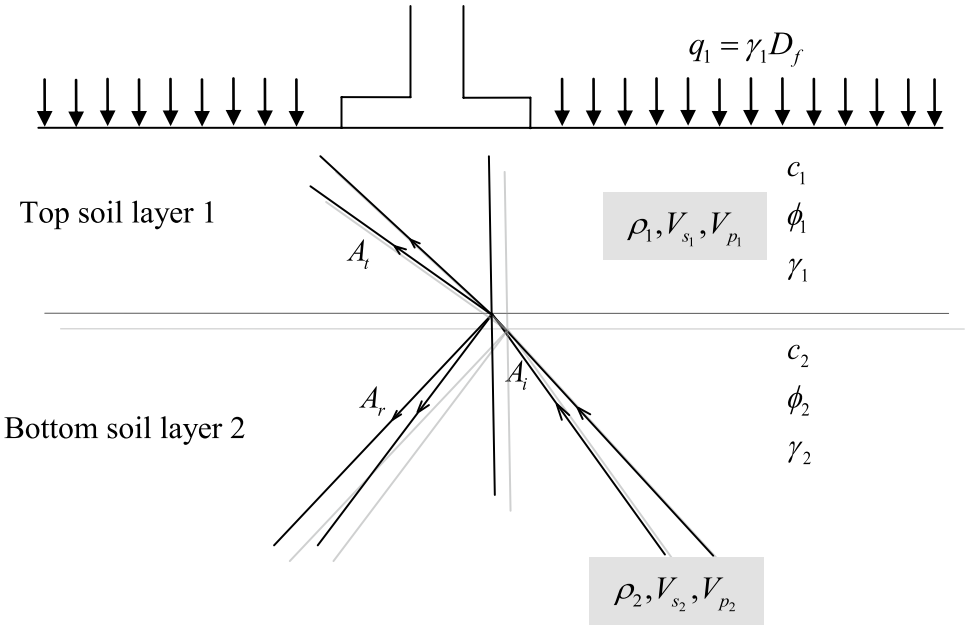

Fig. 3 Wave propagation on two-layered soil

Table 2 Types of wave amplitude and angle with normal plane

Wave type	Velocity	Amplitude	Angle with normal
Incident P	*X*	A	a
Incident S	*Y*	B	b
Incident P	*X*	C	c
Reflected S	*Y*	D	d
Reflected P	*V*	E	e
Reflected S	*Z*	F	f

The equation of motion for stress waves traveling through a visco-elastic medium was first proposed by Yuan et al. (2006). In vector form, the equation may be written as:

$$\rho\frac{\partial^2 u}{\partial t^2} = \left\{(\lambda + G) + (\eta_l + \eta_s)\frac{\partial}{\partial t}\right\}\text{grad}(\kappa) + \left(G + \eta_s\frac{\partial}{\partial t}\right)\nabla^2\bar{u} \tag{3}$$

where ρ = density, λ = Lame constant; G = shear modulus; η_s and η_l = viscosities of the soil; $\bar{u}$ = displacement vector; and κ = div ($\bar{u}$).

The solution of a plane wave propagating vertically in a Kelvin–Voigt homogeneous medium was given by Bellezza (2015) as follows

$$\rho\frac{\partial^2 u_h}{\partial t^2} = G\frac{\partial^2 u_h}{\partial z^2} + \eta_s\frac{\partial^3 u_h}{\partial z^2 \partial t} \tag{4}$$

$$\rho\frac{\partial^2 u_v}{\partial t^2} = (\lambda + 2G)\frac{\partial^2 u_v}{\partial z^2} + (\eta_L + 2\eta_s)\frac{\partial^3 u_v}{\partial z^2 \partial t} \tag{5}$$

The stress–strain relationship of Kelvin–Voigt model is given by

$$\tau = \gamma_s G + \eta_s\frac{\partial \gamma_s}{\partial t} \tag{6}$$

$$\eta_s = \frac{2G\xi}{\omega} \tag{7}$$

where τ = shear stress; γ_s = shear strain; η_s = viscosity of soil; G = shear modulus; ω = angular frequency, ξ = damping ratio.

At the ground surface $z = 0$, shear stress is zero. Assuming a base displacement, the horizontal displacement can be written as:

$$u_{hb} = \frac{u_{h0}}{c_s^2 + s_s^2}\left[(c_s c_{sz} + s_s s_{sz})\cos\omega t + (s_s c_{sz} - c_s s_{sz})\sin\omega t\right] \tag{8}$$

Horizontal acceleration may be obtained by differentiating Eq. (8) twice with respect to time:

$$a_h(z,t) = \frac{k_h g}{c_s^2 + s_s^2}\left[(c_s c_{sz} + s_s s_{sz})\cos\omega t + (s_s c_{sz} - c_s s_{sz})\sin\omega t\right] \tag{9}$$

Similarly, vertical acceleration may be expressed as:

$$a_v(z,t) = \frac{k_h g}{c_p^2 + s_p^2}\left[(c_p c_{pz} + s_p s_{pz})\cos\omega t + (s_p c_{pz} - c_p s_{pz})\sin\omega t\right] \tag{10}$$

H is the total thickness of homogeneous soil layer.

4 Procedure of Analysis

To solve the problem using new pseudo-dynamic method, the following assumptions are made.

a. The soil in each layer is homogeneous and isotropic.
b. The weight of the soil above the base of the foundation has been replaced by a uniform surcharge.
c. The failure mechanism consists of two active wedge angles and passive wedge angles, which are admitted as the variable of this present analysis.

To determine the bearing capacity coefficient, the geometry of the problem is depicted in Figs. 4, 5, 6 and 7. Parameters involved in the present study are as follows:

c_1 = cohesion of soil in top layer, c_2 = cohesion of soil in bottom layer, ϕ_1 = angle of friction of soil in top layer, ϕ_2 = angle of friction of soil in bottom layer, γ_1 = unit weight of soil in top layer,γ_2 = unit weight of soil in bottom layer, ξ_1 = damping ratio in top soil layer, ξ_2 = damping ratio in bottom soil layer, α_{A1} = angle of slip surface at top layer in active zone,α_{A2} = angle of slip surface at bottom layer in active zone,α_{p1} = angle of slip surface at top layer in passive zone,α_{p2} = angle of slip surface at bottom layer in passive zone, δ_1 = friction angle along surface between active and passive zones at the first layer, δ_2 = friction angle along surface between active and passive zones at the second layer. The thickness of the second layer contributing the failure wedge h_2 is expressed as:

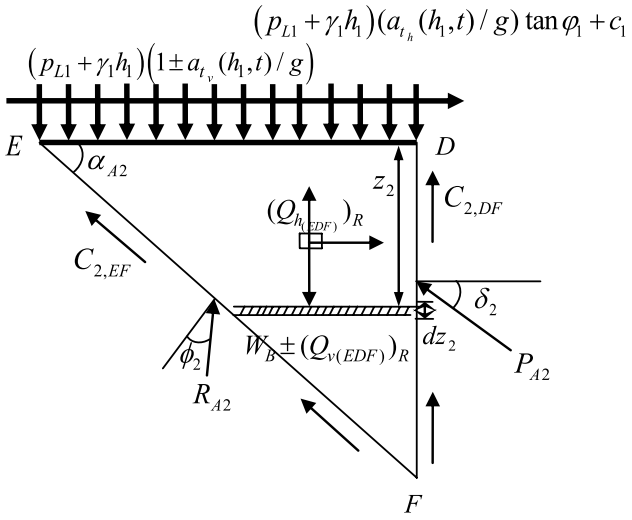

Fig. 5 Active wedge in the bottom layer

$$h_2 = B_0 \tan\alpha_{A2} - h_1 \frac{\tan\alpha_{A2}}{\tan\alpha_{A1}} \quad \text{(Ghazavi and Eghbali 2008)} \tag{11}$$

whereas h_1 is the thickness of first layer.

Active earth pressure and passive resistance in each layer are given, respectively, by:

4.1 Active Pressure at Top Layer

As shown in Fig. 4, wedge ABDE is known as active wedge. The weight of the wedge

$$W_A = \frac{2B_0 - h_1 \cot\alpha_{A1}}{2} h_1 \gamma_1 \tag{12}$$

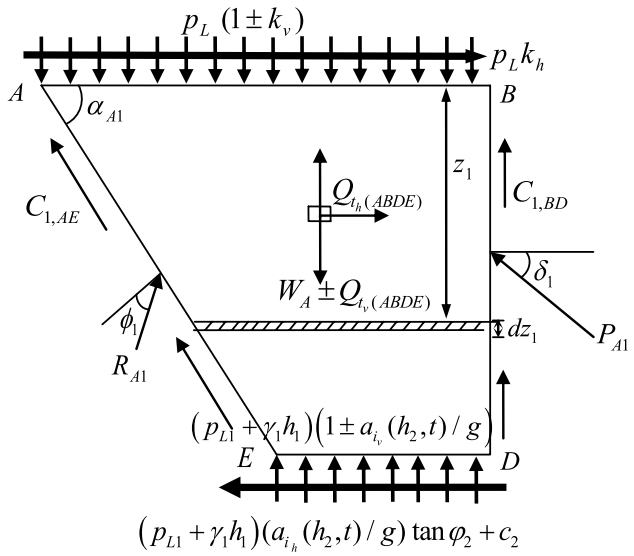

Fig. 4 Active wedge in the top layer

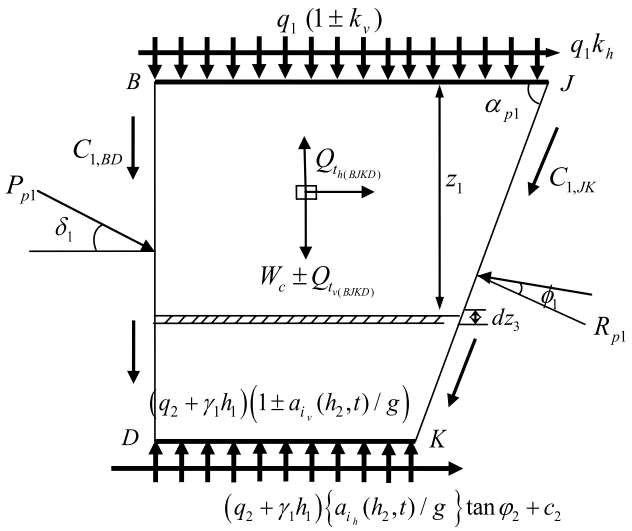

Fig. 6 Passive wedge in the top layer

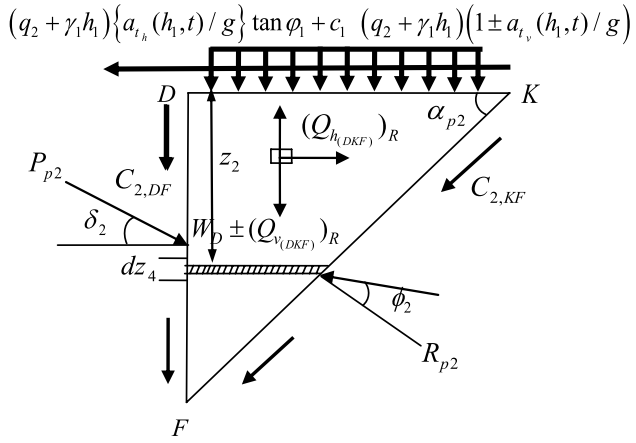

Fig. 7 Passive wedge in the bottom layer

Total load on the foundation is given by

$$P_1 = p_{\mathrm{L}} B_0 \tag{13}$$

Total cohesive force on slip lines BD, AE and ED is given by

$$C_{1,\mathrm{BD}} = c_1 h_1,\ C_{1,\mathrm{AE}} = c_1 \mathrm{AE} = c_1 h_1 \cos ec\,\alpha_{\mathrm{A1}},$$
$$C_{1,\mathrm{ED}} = c_1 \mathrm{ED} = c_1\left(B_0 - h_1 \cot \alpha_{\mathrm{A1}}\right) \tag{14}$$

Considering 2:1 distribution, the intensity of load on the face ED is given by Fig. 8

$$p_{\mathrm{L1}} = \frac{p_{\mathrm{L}} B_0}{\left(B_0 + h_1\right)} \tag{15}$$

The mass of the strip of thickness $\mathrm{d}z_1$ (Fig. 4) in the trapezoidal failure wedge ABDE is given by

$$m(z_1)_{(\mathrm{ABDE})} = \frac{\gamma_1}{g}\left(\frac{B_0 \tan \alpha_{\mathrm{A1}} - z_1}{\tan \alpha_{\mathrm{A1}}}\right) \mathrm{d}z_1 \tag{16}$$

Acceleration of transmitted shear wave is given by:

$$a_{\mathrm{t_h(ABDE)}}(z_1,t) = \frac{a_{\mathrm{t_{h_1}}0}}{c_{\mathrm{s_1}}^2 + s_{\mathrm{s_1}}^2}\left[(c_{\mathrm{s_1}} c_{\mathrm{s_1}z_1} + s_{\mathrm{s_1}} s_{\mathrm{s_1}z_1})\cos\omega t + (s_{\mathrm{s_1}} c_{\mathrm{s_1}z_1} - c_{\mathrm{s_1}} s_{\mathrm{s_1}z_1})\sin\omega t\right] \tag{17}$$

where

$$a_{\mathrm{t_{h_1}}0} = \frac{2}{1+(\alpha_z)_{\mathrm{s}}} a_{\mathrm{i_{h_1}}0};\ a_{\mathrm{i_{h_1}}0} = k_{\mathrm{h}} g;\quad (\alpha_z)_{\mathrm{s}} = \frac{\rho_1 v_{\mathrm{s1}}}{\rho_2 v_{\mathrm{s2}}} \tag{18}$$

From Bellezza (2015), $K_{\mathrm{s_1}}$, $K_{\mathrm{s_2}}$ are the real and imaginary parts of the complex wave no. K_{s}^* is defined as a function of the complex shear modulus G^* in particular $K_{\mathrm{s}}^* = \omega_{\mathrm{s}}\sqrt{\rho/G^*} = K_{\mathrm{s_1}} + iK_{\mathrm{s_2}}$ and $G = G + 2i\xi_1$

$$y_{\mathrm{s_1}} = \frac{\omega_{\mathrm{s}} h_1}{v_{\mathrm{s1}}}\sqrt{\frac{\sqrt{1+4\xi_1^2}+1}{2(1+4\xi_1^2)}} \tag{19}$$

$$y_{\mathrm{s_2}} = -\frac{\omega h_1}{v_{\mathrm{s1}}}\sqrt{\frac{\sqrt{1+4\xi_1^2}-1}{2(1+4\xi_1^2)}} \tag{20}$$

The horizontal inertia force exerted on the small element due to horizontal earthquake acceleration can be expressed as $m(z_1)_{(\mathrm{ABDE})} a_{\mathrm{t_{h(ABDE)}}}(z_1,t)$. The total horizontal inertia force acting in the wedge ABDE may be obtained using the following equations:

$$\begin{aligned} Q_{\mathrm{t_{h(ABDE)}}} &= \int_0^{\mathrm{h_1}} a_{\mathrm{t_{h(ABDE)}}}(z_1,t)\, m(z_1)_{(\mathrm{ABDE})} \\ &= \frac{a_{\mathrm{t_{h_1}}0_{(\mathrm{ABDE})}}\gamma_1}{g\tan\alpha_{A_1}}\left[\frac{c_{\mathrm{s_1}} I_{\mathrm{s_1}} + s_{\mathrm{s_1}} I_{\mathrm{s_2}}}{c_{\mathrm{s_1}}^2 + s_{\mathrm{s_1}}^2}\cos\omega t + \frac{\mathrm{s_{s_1}} I_{\mathrm{s_1}} - c_{\mathrm{s_1}} I_{\mathrm{s_2}}}{c_{\mathrm{s_1}}^2 + s_{\mathrm{s_1}}^2}\sin\omega t\right] \\ &= \frac{a_{\mathrm{t_{h_1}}0_{(\mathrm{ABDE})}}\gamma_1}{g\tan\alpha_{A_1}}\left[A_{\mathrm{h_1}}\cos\omega t + B_{\mathrm{h_1}}\sin\omega t\right] \end{aligned} \tag{21}$$

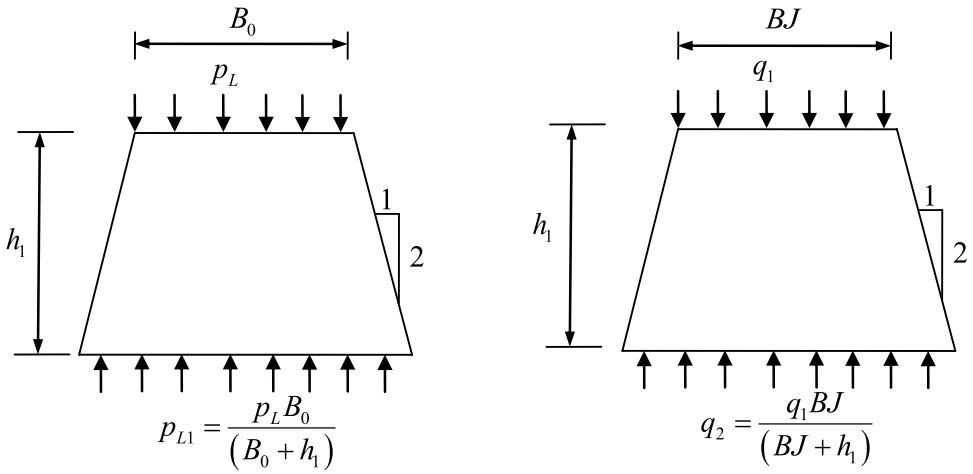

Fig. 8 Load spread mechanism

where $a_{t_{h_1}0} = \frac{2}{1+(\alpha_z)_s} a_{i_{h_1}0}$; $a_{i_{h_1}0} = k_v g$; $(\alpha_z)_s = \frac{\rho_1 v_{s1}}{\rho_2 v_{s2}} A_{h_1}$, B_{h_1} are dimensionless parameters which depend on y_{s_1}, y_{s_2}

Calculation of c_{s_1}, $c_{s_1 z_1}$, s_{s_1}, $s_{s_1 z_1}$, I_{s_1}, I_{s_2}, A_{h_1}, B_{h_1} is given in "Appendix 1".

Similarly, the total vertical inertia force $Q_{t_{v(ABDE)}}$ can be calculated.

Applying limit equilibrium condition, we get,

$$\begin{aligned}&\sum V = 0;\\ &\Rightarrow C_{1,AE}\sin\alpha_{A1} + C_{1,BD} + R_{A1}\cos(\alpha_{A1}-\phi_1) + P_{A1}\sin\delta_1\\ &\quad + \left(p_{L1}+\gamma_1 h_1\right)\mathrm{ED}\left(1 \pm a_{i_v}(h_2,t)/g\right) - P_1(1 \pm k_v) - \left\{W_A + Q_{t_{v(ABDE)}}\right\} = 0\end{aligned} \tag{22}$$

$$\begin{aligned}&\sum H = 0;\\ &\Rightarrow -C_{1,AE}\cos\alpha_{A1} + R_{A1}\sin\left(\alpha_{A1}-\phi_1\right)\\ &\quad - P_{A1}\cos\delta_1 - \left[\left(p_{L1}+\gamma_1 h_1\right)\mathrm{ED}\left(a_{i_h}(h_2,t)/g\right)\tan\phi_2 + c_{2,ED}\mathrm{ED}\right] + P_1 k_h + Q_{t_{h(ABDE)}} = 0\end{aligned} \tag{23}$$

After solving Eqs. 22, 23 and simplifying both, we get the active pressure as given below

$$\begin{aligned}P_{A1} = {} & P_L B_0\left\{\frac{\left\{(1 \pm k_v)\right\}\sin\left(\alpha_{A1}-\phi_1\right) + k_v\cos\left(\alpha_{A1}-\phi_1\right)}{\cos\left(\alpha_{A1}-\phi_1-\delta_1\right)}\right\} - \left\{\frac{p_L B_0}{\left(B_0+h_1\right)}\left(B_0 - h_1\cot\alpha_{A1}\right)\right\}\\ & \left\{\frac{\left(1 \pm a_{i_v}(h_2,t)/g\right)\sin\left(\alpha_{A1}-\phi_1\right) + \left\{a_{i_h}(h_2,t)/g\right\}\tan\phi_2\cos\left(\alpha_{A1}-\phi_1\right)}{\cos\left(\alpha_{A1}-\phi_1-\delta_1\right)}\right\}\\ & + \frac{2B_0 - h_1\cot\alpha_{A1}}{2} h_1\gamma_1\left\{\frac{\sin\left(\alpha_{A1}-\phi_1\right)}{\cos\left(\alpha_{A1}-\phi_1-\delta_1\right)}\right\} - \gamma_1 h_1\left(B_0 - h_1\cot\alpha_{A1}\right)\\ & \left\{\frac{\left(1 \pm a_{i_v}(h_2,t)/g\right)\sin\left(\alpha_{A1}-\phi_1\right) + \left\{a_{i_h}(h_2,t)/g\right\}\tan\phi_2\cos\left(\alpha_{A1}-\phi_1\right)}{\cos\left(\alpha_{A1}-\phi_1-\delta_1\right)}\right\} - 2c_1 h_1\frac{\sin\left(\alpha_{A1}-\phi_1\right)}{\cos\left(\alpha_{A1}-\phi_1-\delta_1\right)}\\ & - c_1 B_0\frac{\cos\left(\alpha_{A1}-\phi_1\right)}{\cos\left(\alpha_{A1}-\phi_1-\delta_1\right)} + Q_{t_{h(ABDE)}}\frac{\cos\left(\alpha_{A1}-\phi_1\right)}{\cos\left(\alpha_{A1}-\phi_1-\delta_1\right)} + Q_{t_{v(ABDE)}}\frac{\sin\left(\alpha_{A1}-\phi_1\right)}{\cos\left(\alpha_{A1}-\phi_1-\delta_1\right)}\end{aligned} \tag{24}$$

4.2 Active Pressure at Bottom Layer

The weight of the wedge EDF

$$W_B = \frac{1}{2}\left(B_0 - h_1\cot\alpha_{A1}\right)h_2\gamma_2 \tag{25}$$

Base shear at the interface between the two layers is given by

$$\left(p_{L1}+\gamma_1 h_1\right)\left\{a_{i_h}(h_2,t)/g\right\}\tan\varphi_2 + c_2,\ \left(p_{L1}+\gamma_1 h_1\right)\left\{a_{t_h}(h_1,t)/g\right\}\tan\varphi_1 + c_1 \tag{26}$$

Total cohesive force at slip lines DF and EF is expressed as given below

$$\begin{aligned}&C_{2,DF} = c_2\mathrm{DF} = c_2 h_2,\ C_{2,EF} = c_2\mathrm{EF} = c_2 h_2\cos ec\alpha_{A2},\\ &C_{1,ED} = c_1\mathrm{ED} = c_1\left(B_0 - h_1\cot\alpha_{A1}\right)\end{aligned} \tag{27}$$

The mass of the strip of thickness dz_2 (Fig. 5) in the triangular failure wedge EDF is given by $m(z_2)_{(EDF)} = \frac{\gamma_2}{g}\left(\frac{h_2 - z_2}{\tan\alpha_{A2}}\right)dz_2$; the acceleration at any depth z_2 below the first soil layer at time t can be expressed as:

$$\begin{aligned}a_{i_{h(EDF)}}(z_2,t) = {} & \frac{a_{i_{h_2}0_{(EDF)}}}{c_{s_2}^2 + s_{s_2}^2}\left[\left(c_{s_2}c_{s_2 z_2} + s_{s_2}s_{s_2 z_2}\right)\cos\omega t\right.\\ & \left.+\left(s_{s_2}c_{s_2 z_2} - c_{s_2}s_{s_2 z_2}\right)\sin\omega t\right]\end{aligned} \tag{28}$$

where

$$c_{s_2z_2} = \cos k_{s_3z_2} \cosh k_{s_4z_2},\ c_{s_2} = \cos y_{s_3} \cosh y_{s_4},\ s_{s_2z_2} = -\sin k_{s_3z_2} \sinh k_{s_4z_2},\ s_{s_2} = -\sin y_{s_3} \sinh y_{s_4}$$
$$= \cos\left(\frac{y_{s_3}z_2}{h_2}\right)\cosh\left(\frac{y_{s_4}z_2}{h_2}\right)$$
$$= -\sin\left(\frac{y_{s_3}z_2}{h_2}\right)\sinh\left(\frac{y_{s_4}z_2}{h_2}\right) \quad (29)$$
$$y_{s_3} = \frac{\omega_s h_2}{v_{s2}}\sqrt{\frac{\sqrt{1+4\xi_2^2}+1}{2(1+4\xi_2^2)}},\ y_{s_4} = -\frac{\omega h_2}{v_{s2}}\sqrt{\frac{\sqrt{1+4\xi_2^2}-1}{2(1+4\xi_2^2)}}$$

Therefore, the total horizontal inertia force $Q_{i_{h(EDF)}}$ acting in the failure wedge EDF is given by

$$Q_{i_{h(EDF)}} = \int_0^{h_2} a_{i_{h(EDF)}}(z_2,t)\,m(z_2)_{(EDF)} = \frac{a_{i_{h_2}0_{(EDF)}}\gamma_2}{g\tan\alpha_{A_2}}\left[A_{h_2}\cos\omega t + B_{h_2}\sin\omega t\right] \quad (30)$$

Horizontal inertia force exerted on the small element due to horizontal reflected earthquake wave acceleration can be expressed as $m(z_2)_{EDF}a_{r_{h(EDF)}}(z_2,t)$. Therefore, the horizontal inertia force $Q_{r_{h(EDF)}}$ acting in the failure wedge EDF is given by

$$Q_{r_{h(EDF)}} = \int_0^{h_2} a_{r_{h(EDF)}}(z_2,t)\,m(z_2)_{(EDF)} \quad (31)$$

$$= \frac{a_{r_{h_2}0_{(EDF)}}\gamma_2}{g\tan\alpha_{A_2}}\left[A_{h_2}\cos\omega t + B_{h_2}\sin\omega t\right] \quad (32)$$

where

$$a_{r_{h_2}0} = \frac{1-(\alpha_z)_s}{1+(\alpha_z)_s}a_{i_{h_2}0};\ a_{i_{h_2}0} = k_h g;\ (\alpha_z)_s = \frac{\rho_1 v_{s1}}{\rho_2 v_{s2}} \quad (33)$$

Net horizontal inertia force

$$(Q_{h_{(EDF)}})_R = Q_{i_{h(EDF)}} - Q_{r_{h(EDF)}} \quad (34)$$

Calculations of I_{s_3}, I_{s_4}, A_{h_2}, B_{h_2} are given in "Appendix 1" Similarly, net vertical inertia force,

$(Q_{v_{(EDF)}})_R$ can be calculated (35)

Applying to limit equilibrium condition,

$$\sum V = 0;$$
$$\Rightarrow C_{2,EF}\sin\alpha_{A2} + C_{2,DF} + R_{A2}\cos(\alpha_{A2}-\phi_2) + P_{A2}\sin\delta_2 - (p_{L1}+\gamma_1 h_1)ED\left\{1 \pm a_{t_v}(h_1,t)/g\right\} - \left\{W_B + (Q_{v_{(EDF)}})R\right\} = 0 \quad (36)$$

$$\sum H = 0;$$
$$\Rightarrow C_{1,ED} - C_{2,EF}\cos\alpha_{A2} + R_{A2}\sin(\alpha_{A2}-\phi_2) - P_{A2}\cos\delta_2 + (p_{L1}+\gamma_1 h_1)ED\left\{a_{t_h}(h_1,t)/g\right\}\tan\phi_1 + (Q_{h_{(EDF)}})_R = 0 \quad (37)$$

Solving Eqs. 36, 37 and simplifying, we get

$$P_{A2} = \frac{p_L B_0}{B_0+h_1}(B_0 - h_1\cot\alpha_{A1})\left\{\frac{(1\pm a_{t_v}(h_1,t)/g)\sin(\alpha_{A2}-\phi_2) + \{a_{t_h}(h_1,t)/g\}\tan\phi_1\cos(\alpha_{A2}-\phi_2)}{\cos(\alpha_{A2}-\phi_2-\delta_2)}\right\}$$
$$+ \frac{1}{2}(B_0 - h_1\cot\alpha_{A1})h_2\gamma_2\left\{\frac{\sin(\alpha_{A2}-\phi_2)}{\cos(\alpha_{A2}-\phi_2-\delta_2)}\right\} + \gamma_1 h_1(B_0 - h_1\cot\alpha_{A1})$$
$$\left\{\frac{(1\pm a_{t_v}(h_1,t)/g)\sin(\alpha_{A2}-\phi_2) + \{a_{t_h}(h_1,t)/g\}\tan\phi_1\cos(\alpha_{A2}-\phi_2)}{\cos(\alpha_{A2}-\phi_2-\delta_2)}\right\} - 2c_2h_2\frac{\sin(\alpha_{A2}-\phi_2)}{\cos(\alpha_{A2}-\phi_2-\delta_2)} \quad (38)$$
$$- c_2h_2\cot\alpha_{A2}\frac{\cos(\alpha_{A2}-\phi_2)}{\cos(\alpha_{A2}-\phi_2-\delta_2)} - c_1\left[h_1\cot\alpha_{A1}\frac{\cos(\alpha_{A2}-\phi_2)}{\cos(\alpha_{A2}-\phi_2-\delta_2)} - B_0\frac{\cos(\alpha_{A2}-\phi_2)}{\cos(\alpha_{A2}-\phi_2-\delta_2)}\right]$$
$$+ (Q_{h_{(EDF)}})_R\frac{\cos(\alpha_{A2}-\phi_2)}{\cos(\alpha_{A2}-\phi_2-\delta_2)} + (Q_{v_{(EDF)}})_R\frac{\sin(\alpha_{A2}-\phi_2)}{\cos(\alpha_{A2}-\phi_2-\delta_2)}$$

Total active pressure from both the layers is given by

$$P_{\mathrm{A}} = P_{\mathrm{A1}} + P_{\mathrm{A2}} \tag{39}$$

4.3 Passive Resistance at Top Layer

Due to active pressure generated in top layer, passive zone provides the resistance to prevent the movement toward that direction. The weight of the passive wedge BJKD (Fig. 6)

$$W_{\mathrm{c}} = \frac{\mathrm{h}_1 \cot\alpha_{p1} + 2h_2 \cot\alpha_{\mathrm{p2}}}{2} h_1\gamma_1 \tag{40}$$

Total surcharge load in top layer of passive zone

$$\begin{aligned} Q_1 &= q_1 \mathrm{BJ} \\ &= \gamma_1 D_{\mathrm{f}}(h_1 \cot\alpha_{p1} + h_2 \cot\alpha_{\mathrm{p2}}) \end{aligned} \tag{41}$$

Total cohesive force in slip lines BD and JK of passive wedge

$$C_{1,DK} = c_1 DK = c_1 h_2 \cot\alpha_{\mathrm{p2}},\ C_{1,BD} = c_1 BD = c_1 h_1,\ C_{1,JK} = c_1 JK = c_1 h_1 \cos ec\alpha_{p1} \tag{42}$$

The mass of the strip of thickness $\mathrm{d}z_1$(Fig. 6) in the trapezoidal failure wedge BJKD is given by $m(z_1)_{\mathrm{BJKD}} = \frac{\gamma_1}{g}(h_1 \cot\alpha_{p1} + h_2 \cot\alpha_{\mathrm{p2}} - z_1 \cot\alpha_{p1})\mathrm{d}z_1$, the acceleration at any depth z_1 below the ground surface and time t can be expressed as:

$$a_{\mathrm{t_{h(BJKD)}}}(z_1,t) = \frac{a_{\mathrm{t_{h_1}0_{(BJKD)}}}}{c_{\mathrm{s_3}}^2 + s_{\mathrm{s_3}}^2}\left[(c_{\mathrm{s_3}} c_{\mathrm{s_3}z_1} + s_{\mathrm{s_3}} s_{\mathrm{s_3}z_1})\cos\omega t + (s_{\mathrm{s_3}} c_{\mathrm{s_3}z_1} - c_{\mathrm{s_3}} s_{\mathrm{s_3}z_1})\sin\omega t\right] \tag{43}$$

where

$$\begin{aligned} c_{\mathrm{s_3}z_1} &= \cos k_{\mathrm{s_5}z_1} \cosh k_{\mathrm{s_6}z_1} \\ &= \cos\left(\frac{y_{\mathrm{s_5}} z_1}{\mathrm{h}_1}\right)\cosh\left(\frac{y_{\mathrm{s_6}} z_1}{\mathrm{h}_1}\right) \\ c_{\mathrm{s_3}} &= \cos y_{\mathrm{s_5}} \cosh y_{\mathrm{s_6}} \\ s_{\mathrm{s_3}z_1} &= -\sin k_{\mathrm{s_5}z_1} \sinh k_{\mathrm{s_6}z_1} \\ &= -\sin\left(\frac{y_{\mathrm{s_5}} z_1}{\mathrm{h}_1}\right)\sinh\left(\frac{y_{\mathrm{s_6}} z_1}{\mathrm{h}_1}\right) s_{\mathrm{s_3}z_1} = -\sin k_{\mathrm{s_5}z_1} \sinh k_{\mathrm{s_6}z_1} \\ &= -\sin\left(\frac{y_{\mathrm{s_5}} z_1}{\mathrm{h}_1}\right)\sinh\left(\frac{y_{\mathrm{s_6}} z_1}{\mathrm{h}_1}\right) \end{aligned}$$

$$s_{\mathrm{s_3}} = -\sin y_{\mathrm{s_5}} \sinh y_{\mathrm{s_6}}$$

$$y_{\mathrm{s_5}} = \frac{\omega_{\mathrm{s}} h_1}{v_{\mathrm{s1}}}\sqrt{\frac{\sqrt{1+4\xi_1^2}+1}{2(1+4\xi_1^2)}},\quad y_{\mathrm{s_6}} = -\frac{\omega_{\mathrm{s}} h_1}{v_{\mathrm{s1}}}\sqrt{\frac{\sqrt{1+4\xi_1^2}-1}{2(1+4\xi_1^2)}}, \tag{44}$$

The horizontal—due to horizontal earthquake acceleration—can be expressed as $m(z_1)_{\mathrm{BJKD}} a_{\mathrm{t_{h(BJKD)}}}(z_1,t)$. Therefore, the total horizontal inertia force $Q_{\mathrm{t_{h(BJKD)}}}$ acting in the failure wedge *BJKD* is given by

$$\begin{aligned} Q_{\mathrm{t_{h(BJKD)}}} &= \int_0^{\mathrm{h}_2} a_{\mathrm{t_{h(BJKD)}t_{h(BJKD)}}}(z_1,t) m(z_1)_{\mathrm{(BJKD)}} \\ &= \frac{a_{\mathrm{t_{h_1}0_{(BJKD)}}}\gamma_2}{g\tan\alpha_{p_2}}\left[A_{\mathrm{h_3}}\cos\omega t + B_{\mathrm{h_3}}\sin\omega t\right] \end{aligned} \tag{45}$$

where

$$a_{\mathrm{t_{h_1}}0} = \frac{2}{1+(\alpha_z)_{\mathrm{s}}} a_{\mathrm{i_{h_1}}0};\quad a_{\mathrm{i_{h_1}}0} = k_{\mathrm{h}} g;\ (\alpha_z)_{\mathrm{s}} = \frac{\rho_1 v_{\mathrm{s1}}}{\rho_2 v_{\mathrm{s2}}} \tag{46}$$

Detailed calculations of $I_{\mathrm{s_5}}$,$I_{\mathrm{s_6}}$,$A_{\mathrm{h_3}}$, $B_{\mathrm{h_3}}$ are given in "Appendix 2".

Similarly, the total vertical inertia force, $Q_{\mathrm{t_{v(BJKD)}}}$ acting in the failure wedge BJKD can be evaluated.

Using limit equilibrium condition,

$$\begin{aligned} &\sum V = 0; \\ &\Rightarrow -C_{1,\mathrm{BD}} - C_{1,\mathrm{JK}}\sin\alpha_{p1} + R_{p1}\cos\left(\phi_1 + \alpha_{\mathrm{p1}}\right) \\ &\quad - P_{\mathrm{p1}}\sin\delta_1 + \left(q_2 + \gamma_1 h_1\right)\mathrm{DK}\left\{1 \pm a_{\mathrm{i_v}}(h_2,t)/g\right\} \\ &\quad - \left(Q_1\right)\left\{1 \pm k_{\mathrm{v}}\right\} - \left\{W_{\mathrm{c}} + Q_{\mathrm{t_{v(BJKD)}}}\right\} = 0 \end{aligned} \tag{47}$$

$$\sum H = 0;$$
$$\Rightarrow -C_{1,\mathrm{JK}}\cos\alpha_{\mathrm{p1}} + C_{1,\mathrm{DK}} - R_{\mathrm{p1}}\sin\left(\phi_1+\alpha_{\mathrm{p1}}\right) + P_{\mathrm{p1}}\cos\delta_1 + \left(q_2+\gamma_1 h_1\right)\mathrm{DK}\left\{a_{\mathrm{i_h}}(h_2,t)/g\right\}\tan\phi_2 + Q_1 k_{\mathrm{h}} + Q_{\mathrm{t_{h(BJKD)}}} = 0 \tag{48}$$

Solving Eqs. 47, 48 and after simplification, passive resistance can be expressed as:

$$\begin{aligned}-P_{\mathrm{p1}} = {}& \frac{\mathrm{h}_1\cot\alpha_{p1}+2h_2\cot\alpha_{\mathrm{p2}}}{2}h_1\gamma_1\left\{\frac{\sin\left(\phi_1+\alpha_{p1}\right)}{\cos\left(\phi_1+\alpha_{p1}+\delta_1\right)}\right\} - \gamma_1 h_1 h_2\cot\alpha_{\mathrm{p2}}\\ & \left\{\frac{\left\{1\pm a_{\mathrm{i_v}}(h_2,t)/g\right\}\sin\left(\phi_1+\alpha_{p1}\right)+\left\{a_{\mathrm{i_h}}(h_2,t)/g\right\}\tan\phi_2\cos\left(\phi_1+\alpha_{p1}\right)}{\cos\left(\phi_1+\alpha_{p1}+\delta_1\right)}\right\}\\ & -\gamma_1 D_{\mathrm{f}}\frac{\left(\mathrm{h}_1\cot\alpha_{p1}+h_2\cot\alpha_{\mathrm{p2}}\right)}{\left(\mathrm{h}_1+h_1\cot\alpha_{p1}+h_2\cot\alpha_{\mathrm{p2}}\right)}h_2\cot\alpha_{\mathrm{p2}}\\ & \left\{\frac{1\pm a_{\mathrm{i}}v(h_2,t)/g\sin\left(\phi_1+\alpha_{p1}\right)+a_{\mathrm{i_h}}h(h_2,t)/g\tan\phi_2\cos\left(\phi_1+\alpha_{p1}\right)}{\cos\left(\phi_1+\alpha_{p1}+\delta_1\right)}\right\}+\gamma_1 D_{\mathrm{f}}\left(\mathrm{h}_1\cot\alpha_{\mathrm{p1}}+h_2\cot\alpha_{\mathrm{p2}}\right)\\ & \left\{\frac{\left(1\pm k_{\mathrm{v}}\right)\sin\left(\phi_1+\alpha_{\mathrm{p1}}\right)-k_{\mathrm{h}}\cos\left(\phi_1+\alpha_{\mathrm{p1}}\right)}{\cos\left(\phi_1+\alpha_{\mathrm{p1}}+\delta_1\right)}\right\}+2c_1h_1\left\{\frac{\sin\left(\phi_1+\alpha_{p1}\right)}{\cos\left(\phi_1+\alpha_{\mathrm{p1}}+\delta_1\right)}\right\}\\ & +c_1\left[\mathrm{h}_1\cot\alpha_{\mathrm{p1}}\left\{\frac{\cos\left(\phi_1+\alpha_{\mathrm{p1}}\right)}{\cos\left(\phi_1+\alpha_{\mathrm{p1}}+\delta_1\right)}\right\}-h_2\cot\alpha_{\mathrm{p2}}\left\{\frac{\cos\left(\phi_1+\alpha_{\mathrm{p1}}\right)}{\cos\left(\phi_1+\alpha_{\mathrm{p1}}+\delta_1\right)}\right\}\right]\\ & -Q_{\mathrm{t_{h(BJKD)}}}\frac{\cos\left(\phi_1+\alpha_{\mathrm{p1}}\right)}{\cos\left(\phi_1+\alpha_{\mathrm{p1}}+\delta_1\right)}+Q_{\mathrm{t_{v(BJKD)}}}\frac{\sin\left(\phi_1+\alpha_{\mathrm{p1}}\right)}{\cos\left(\phi_1+\alpha_{\mathrm{p1}}+\delta_1\right)}\end{aligned} \tag{49}$$

4.4 Passive Resistance at Bottom Layer

Total weight of the passive wedge DKF is shown in Fig. 7

$$W_{\mathrm{D}} = \frac{1}{2}h_2^2\cot\alpha_{\mathrm{p2}}\gamma_2 \tag{50}$$

According to 2 : 1, load distribution method intensity of surcharge load at depth h_1 can be written (Fig. 8)

$$q_2 = \frac{q_1\mathrm{DK}}{\left(\mathrm{DK}+h_1\right)} = \frac{q_1\left(\mathrm{h}_1\cot\alpha_{p1}+h_2\cot\alpha_{\mathrm{p2}}\right)}{\left(\mathrm{h}_1+h_1\cot\alpha_{p1}+h_2\cot\alpha_{\mathrm{p2}}\right)} \tag{51}$$

Base shear between two passive wedges can be written as

$$\begin{aligned}&\left(q_2+\gamma_1 h_1\right)\left\{a_{\mathrm{i_h}}(h_2,t)/g\right\}\ \tan\phi_2 + c_2,\\ &\left(q_2+\gamma_1 h_1\right)\left\{a_{\mathrm{t_h}}(h_1,t)/g\right\}\ \tan\phi_1 + c_1,\end{aligned} \tag{52}$$

Cohesive forces in slip lines DF, KF and DK are given by, respectively

$C_{2,\mathrm{DF}} = c_2\mathrm{DF} = c_2h_2,\ C_{2,\mathrm{KF}} = c_2\mathrm{KF} = c_2h_2\cos ec\alpha_{\mathrm{p2}},$
$C_{1,\mathrm{DK}} = c_1h_2\cot\alpha_{\mathrm{p2}}$

The mass of the strip of thickness $\mathrm{d}z_4$ (Fig. 7) in the triangular failure wedge DKF is given by $m(z_4)_{\mathrm{DKF}} = \frac{\gamma_2}{g}\left(C_{1,DK} = c_1h_2\cot\alpha_{\mathrm{p2}}\right)\mathrm{d}z_4$, the acceleration at any depth z_4 below the first soil layer and time can be expressed as:

$$\begin{aligned}\mathrm{a}_{\mathrm{i_{h(DKF)}}}(z_2,t) = {}& \frac{a_{\mathrm{i_{h_2}0_{(DKF)}}}}{c_{\mathrm{s_4}}^2+s_{\mathrm{s_4}}^2}\left[\left(c_{\mathrm{s_4}}c_{\mathrm{s_4}z_2}+s_{\mathrm{s_4}}s_{\mathrm{s_4}z_2}\right)\cos\omega t\right.\\ & \left.+\left(s_{\mathrm{s_4}}c_{\mathrm{s_4}z_2}-c_{\mathrm{s_4}}s_{\mathrm{s_4}z_2}\right)\sin\omega t\right]\end{aligned} \tag{53}$$

where

$$\begin{aligned}c_{\mathrm{s_4}z_2} &= \cos k_{\mathrm{s_7}z_2}\cosh k_{\mathrm{s_8}z_2}\\ &= \cos\left(\frac{y_{\mathrm{s_7}}z_2}{\mathrm{h}_2}\right)\cosh\left(\frac{y_{\mathrm{s_8}}z_2}{\mathrm{h}_2}\right),\ c_{\mathrm{s_4}} = \cos y_{\mathrm{s_7}}\cosh y_{\mathrm{s_8}}\\ s_{\mathrm{s_4}z_2} &- \sin\left(\frac{y_{\mathrm{s_7}}z_2}{\mathrm{h}_2}\right)\sinh\left(\frac{y_{\mathrm{s_8}}z_2}{\mathrm{h}_2}\right),\ s_{\mathrm{s_4}} = -\sin y_{\mathrm{s_7}}\sinh y_{\mathrm{s_8}}\\ y_{\mathrm{s_7}} &= \frac{\omega_{\mathrm{s}}h_2}{v_{\mathrm{s2}}}\sqrt{\frac{\sqrt{1+4\xi_2^2}+1}{2(1+4\xi_2^2)}},\ y_{\mathrm{s_8}} = -\frac{\omega h_2}{v_{\mathrm{s2}}}\sqrt{\frac{\sqrt{1+4\xi_2^2}-1}{2(1+4\xi_2^2)}}\end{aligned}$$

The horizontal inertia force exerted on the small element due to horizontal incidental shear wave acceleration can be expressed as $m(z_2)_{\mathrm{DKF}} a_{\mathrm{i_{h(DKF)}}}(z_2,t)$. Therefore, the total horizontal inertia force $Q_{ih_{(DKF)}}$ acting in the failure wedge EDF is given by

$$\begin{aligned} Q_{\mathrm{i_{h(DKF)}}} &= \int_0^{\mathrm{h_2}} a_{\mathrm{i_{h(DKF)}}}(z_2,t) m(z_2)_{\mathrm{(DKF)}} \\ &= \frac{a_{\mathrm{i_{h2}0_{(DKF)}}}\gamma_2}{g\tan\alpha_{\mathrm{p_2}}}\left[\frac{c_{\mathrm{s_4}} I_{\mathrm{s_7}} + s_{\mathrm{s_4}} I_{\mathrm{s_8}}}{c_{\mathrm{s_4}}^2 + s_{\mathrm{s_4}}^2}\cos\omega t + \frac{\mathrm{s_{s_4}} I_{\mathrm{s_7}} 7 - c_{\mathrm{s_4}} I_{\mathrm{s_8}}}{c_{\mathrm{s_4}}^2 + s_{\mathrm{s_4}}^2}\sin\omega t\right] \\ &= \frac{a_{\mathrm{i_{h2}0_{(DKF)}}}\gamma_2}{g\tan\alpha_{\mathrm{p_2}}}\left[A_{\mathrm{h_4}}\cos\omega t + B_{\mathrm{h_4}}\sin\omega t\right] \end{aligned} \tag{54}$$

The horizontal inertia force exerted on the small element due to reflected shear wave acceleration can be expressed as:

$$\begin{aligned} Q_{\mathrm{r}_{h(DKF)}} &= \int_0^{\mathrm{h_2}} a_{\mathrm{r_{h(DKF)}}}(z_2,t) m(z_2)_{\mathrm{(DKF)}} \\ &= \frac{a_{\mathrm{r_{h2}0_{(DKF)}}}\gamma_2}{g\tan\alpha_{\mathrm{p_2}}}\left[A_{\mathrm{h_4}}\cos\omega t + B_{\mathrm{h_4}}\sin\omega t\right] \end{aligned} \tag{55}$$

where $a_{\mathrm{r_{h_2}}0} = \frac{1-(\alpha_z)_{\mathrm{s}}}{1+(\alpha_z)_{\mathrm{s}}} a_{\mathrm{i_{h_2}}0}$; $a_{\mathrm{i_{h_2}}0} = k_h g$; $(\alpha_z)_{\mathrm{s}} = \frac{\rho_1 v_{s1}}{\rho_2 v_{s2}}$

Net horizontal inertia force

$$(Q_{\mathrm{h_{(DKF)}}})_{\mathrm{R}} = Q_{\mathrm{i_{h(DKF)}}} - Q_{\mathrm{r_{h(DKF)}}} \tag{56}$$

Detailed calculation of equations $I_{\mathrm{s_7}}$, $I_{\mathrm{s_8}}$, $A_{\mathrm{h_4}}$, $B_{\mathrm{h_4}}$ is given in "Appendix 2"

Similarly, the net vertical inertia force $(Q_{\mathrm{v}_{(DKF)}})_{\mathrm{R}}$ can be calculated

Applying equilibrium conditions,

$$\begin{aligned} &\textstyle\sum V = 0; \\ &\Rightarrow\ -C_{2,\mathrm{DF}} - C_{2,\mathrm{KF}}\sin\alpha_{\mathrm{p2}} + R_{\mathrm{p2}}\cos\left(\phi_2 + \alpha_{\mathrm{p2}}\right) - P_{\mathrm{p2}}\sin\delta_2 - \left(q_2 + \gamma_1 h_1\right)\mathrm{DK}\left\{1 \pm a_{\mathrm{t_v}}(h_1,t)/g\right\} - \left\{W_{\mathrm{D}} + (Q_{\mathrm{v_{(DKF)}}})_{\mathrm{R}}\right\} = 0 \end{aligned} \tag{57}$$

$$\begin{aligned} &\textstyle\sum H = 0; \\ &\Rightarrow -C_{1,\mathrm{DK}} - C_{2,\mathrm{KF}}\cos\alpha_{\mathrm{p2}} - R_{\mathrm{p2}}\sin\left(\phi_2 + \alpha_{\mathrm{p2}}\right) + P_{\mathrm{p2}}\cos\delta_2 - \left(q_2 + \gamma_1 h_1\right)\mathrm{DK}\left\{a_{\mathrm{t_h}}(h_1,t)/g\right\}\tan\phi_1 + (Q_{\mathrm{h_{(DKF)}}})_{\mathrm{R}} = 0 \end{aligned} \tag{58}$$

Solving Eqs. (57) and (58), it can be expressed as

$$\begin{aligned} P_{\mathrm{p2}} &= \frac{1}{2}h_2^2\cot\alpha_{\mathrm{p2}}\gamma_2\left\{\frac{\sin\left(\phi_2+\alpha_{\mathrm{p2}}\right)}{\cos\left(\phi_2+\alpha_{\mathrm{p2}}+\delta_2\right)}\right\} + \gamma_1 h_1 h_2\cot\alpha_{\mathrm{p2}} \\ &\left\{\frac{\left\{1 \pm a_{t_v}(h_1,t)/g\right\}\sin\left(\phi_2+\alpha_{\mathrm{p2}}\right) + \left\{a_{\mathrm{t_h}}(h_1,t)/g\right\}\tan\phi_1\cos\left(\phi_2+\alpha_{\mathrm{p2}}+\delta_2\right)}{\cos\left(\phi_2+\alpha_{\mathrm{p2}}\right)}\right\} \\ &+ \gamma_1 D_{\mathrm{f}}\frac{\left(\mathrm{h}_1\cot\alpha_{\mathrm{p1}} + h_2\cot\alpha_{\mathrm{p2}}\right)}{\left(\mathrm{h}_1 + h_1\cot\alpha_{\mathrm{p1}} + h_2\cot\alpha_{\mathrm{p2}}\right)}h_2\cot\alpha_{\mathrm{p2}} \\ &\left\{\frac{\left\{1 \pm a_{\mathrm{t_v}}(h_1,t)/g\right\}\sin\left(\phi_2+\alpha_{\mathrm{p2}}\right) + \left\{a_{\mathrm{t_v}}(h_1,t)/g\right\}\tan\phi_1\cos\left(\phi_2+\alpha_{\mathrm{p2}}\right)}{\cos\left(\phi_2+\alpha_{\mathrm{p2}}+\delta_2\right)}\right\} \\ &+ 2c_2 h_2\left\{\frac{\sin\left(\phi_2+\alpha_{\mathrm{p2}}\right)}{\cos\left(\phi_2+\alpha_{\mathrm{p2}}+\delta_2\right)}\right\} + c_1 h_2\cot\alpha_{\mathrm{p2}}\left\{\frac{\cos\left(\phi_2+\alpha_{\mathrm{p2}}\right)}{\cos\left(\phi_2+\alpha_{\mathrm{p2}}+\delta_2\right)}\right\} \\ &+ c_2 h_2\cot\alpha_{\mathrm{p2}}\left\{\frac{\cos\left(\phi_2+\alpha_{\mathrm{p2}}\right)}{\cos\left(\phi_2+\alpha_{\mathrm{p2}}+\delta_2\right)}\right\} + (Q_{\mathrm{v_{(DKF)}}})_{\mathrm{R}}\frac{\sin\left(\phi_2+\alpha_{\mathrm{p2}}\right)}{\cos\left(\phi_2+\alpha_{\mathrm{p2}}+\delta_2\right)} \\ &- (Q_{\mathrm{h_{(DKF)}}})_{\mathrm{R}}\frac{\cos\left(\phi_2+\alpha_{\mathrm{p2}}\right)}{\cos\left(\phi_2+\alpha_{\mathrm{p2}}+\delta_2\right)} \end{aligned} \tag{59}$$

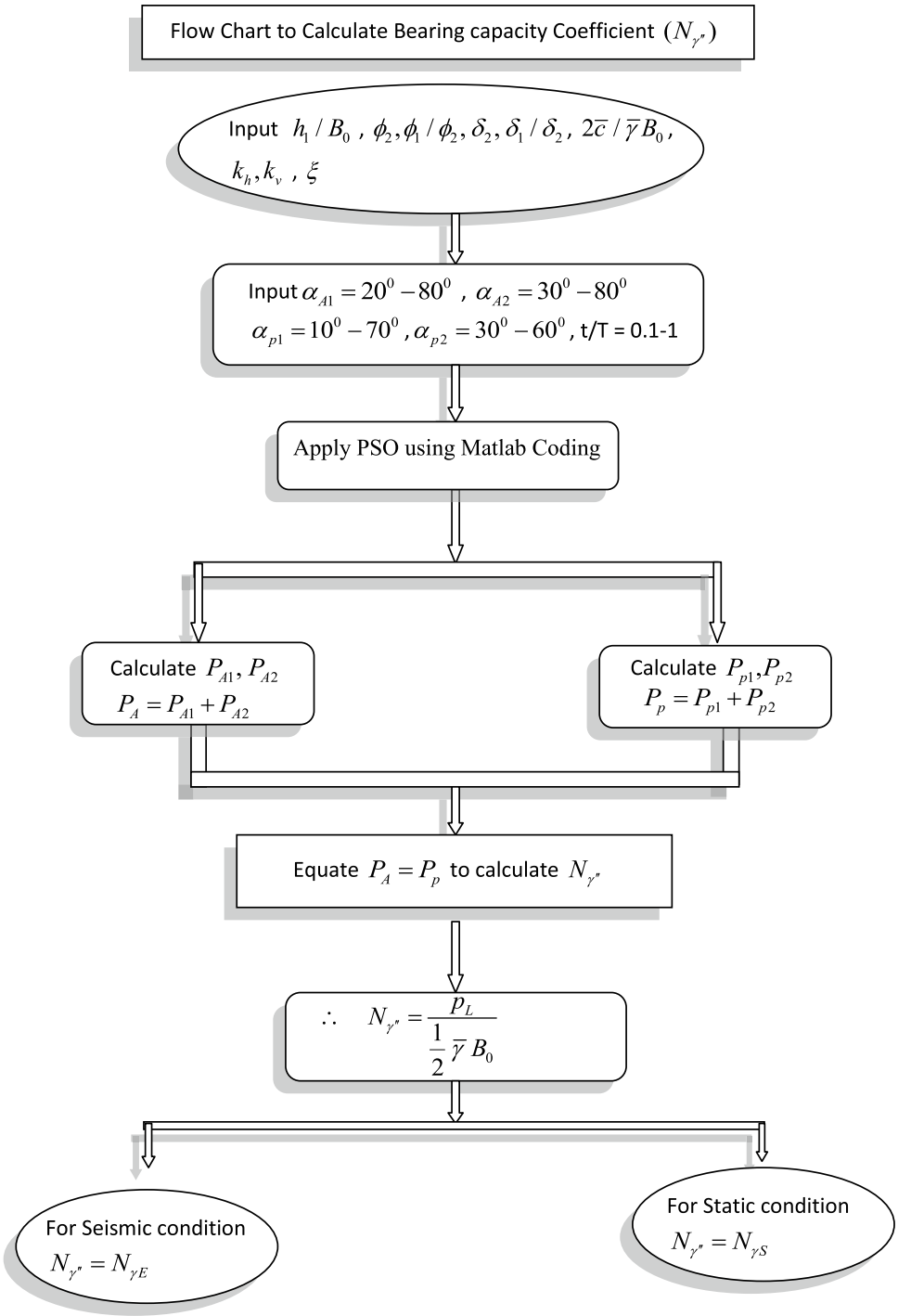

Fig. 9 Flowchart to calculate bearing capacity coefficient $N_{\gamma''}$

Total passive resistance from the two wedges can be expressed as

$$P_{\mathrm{p}} = P_{p1} + P_{\mathrm{p2}} \tag{60}$$

In Fig. 2, it is seen that line BF can be thought as a retaining wall with the total active lateral thrust P_{A} from two layers of soil pushing against the passive resistance P_{p}. At equilibrium, the components of two active force and passive resistance are equal. Thus, equating Eqs. 39 and 60, the final expression reduces to the form of Eq. 62

$$P_{\mathrm{A}} = P_{\mathrm{p}} \tag{61}$$

$$p_{\mathrm{L}} = \frac{1}{2}\bar{\gamma} N_{\gamma''} \tag{62}$$

$N_{\gamma''}$ is a single bearing capacity coefficient for the simultaneous resistance of cohesion, unit weight and surcharge. In seismic condition, $N_{\gamma''}$ is expressed as $N_{\gamma E}$ and static condition $N_{\gamma S}\bar{\gamma}$ is the equivalent unit weight and is given by,

$$\bar{\gamma} = \frac{A_1\gamma_1 + A_2\gamma_2}{A_1 + A_2} \tag{63}$$

where A_1 and A_2 are the effective area of each layer in breach zone and dependent on h_1 and h_2. Bearing capacity coefficient ($N_{\gamma''}$) is a function of several parameters including cohesion, surcharge and unit weight. It can be expressed as

$$N_{\gamma''} = \left(\frac{a_1}{e_1} + \frac{b_1}{e_1} + \frac{2\bar{c}}{\bar{\gamma}B_0}\,\frac{d_1}{e_1}\right) \tag{64}$$

where $\bar{c}$ is defined as the weighted averaged cohesion showing the proportion of each layer in the slip line and is given by

$$\bar{c} = \frac{c_1h_1 + c_2h_2}{\mathrm{h}_1 + h_2} \tag{65}$$

The detail equations for a_1, b_1, d_1 and e_1 are given in "Appendix 3", and the flowchart of the present methodology is shown in Fig. 9.

Since the heuristic algorithms give us low ramification and high execution, these methods are relatively new and can be applied in the geotechnical problem. Out of these methods, a brief discussion on particle swarm optimization is given here as it is used in the analysis.

5 Particle Swarm Optimization

Kennedy and Eberhart (1995) have developed PSO as a stimulation of birds swarm. Swarm is a group of individuals with defined rules for individual behaviors and communications. The ability of each individual to deal with the previous experiences of the swarm is called swarm intelligence. This capability guides the swarm toward its optimum goal. PSO is a population-based search technique where a population of particles starts their journey in a space with respect to the current best position (Hossain and El-Shafie 2014). Reynolds (1987) described three simple rules for the behavior of individuals inside a swarm which are used as one of the basic concepts of PSO by Kennedy and Eberhart (1995). Although these simple rules model the behavior of individuals, their combination produces a complicated behavior for the swarm:

a. Individuals avoid collision with others
b. Individuals go toward the goal of swarm
c. Individuals go to the center of swarm

The process of decision making related to individuals is other basic concept of PSO. Each individual of the swarm makes decision based on the following two factors:

1. The own experiences of individual that is its best results so far 2. The experiences of other individuals in the swarm that is the best results in the whole swarm. Figure 10 illustrates one flowchart to optimize a problem using PSO. At the starting step of the original PSO, a certain number of individuals, called particles, are distributed in the search space by using a random pattern (Kennedy and Eberhart 1995; Cheng et al. 2007). Each particle is a representative of a feasible solution. Figure 11 shows the schematic structure of a particle in PSO involving three divided parts as its current position, best position, and velocity. The current position, best position and velocity of particles record, respectively, the current coordinates, best coordinates and velocity vectors of a particle in D-dimensional space, where D starts from one (Kalatehjari 2013). Consequently, for a particle in D-dimensional space, a 3-dimensional particle

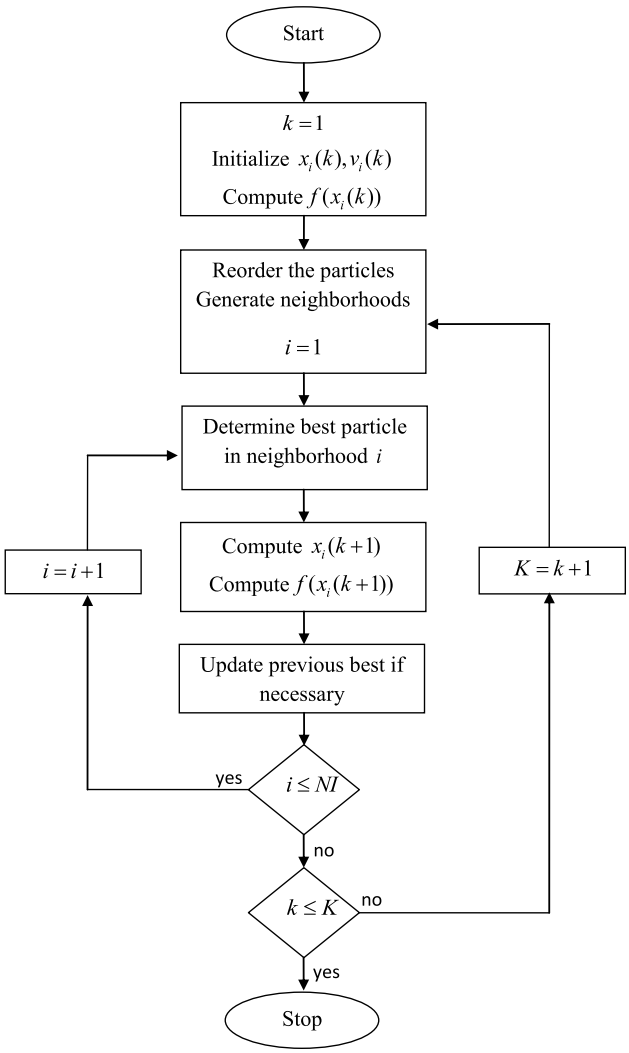

Fig. 10 Flowchart of PSO algorithm

is desirable. The aim of PSO is to meet the termination criteria which are defined as the criteria for terminating the iterative search process. To select an appropriate termination criterion, it should be noted that the termination condition does not cause a prematurely converge and it should protect against oversampling of the fitness (Engelbrecht 2007). The following termination criteria are frequently used in PSO: 1. Termination when the maximum number of iterations is exceeded 2. Termination when a satisfactory solution is found based on the condition of each problem 3. Termination when no improvement is achieved over a certain number of iterations. These criteria are applied to ensure that PSO is able to converge on a feasible solution. In fact, PSO tries to make the objective function as minimum or maximum depend to the problem to be solved. To lead the swarm toward this aim, the fitness value of each particle is determined by evaluating its current position by the objective function. After evaluating the fitness of all particles, Eq. 66 (velocity equation) is used to calculate the velocity of particles based on their best position and the position of the best particle in the swarm. Using Eq. 67, particle positions can be updated according to their current positions and velocities. This iterative process continues until reaching the termination criteria. Equations 66 and 67 are as follows (Kennedy and Eberhart 1995):

Let X and V denote a particle's position and velocity in a search space. Then, the ith particle can be interpreted as $X_i = (x_{i1}, x_{i2}, x_{i3,} \ldots \ldots \ldots \ldots \ldots, x_{id})$ and the velocity of the ith particle is delimited by $V_i = \left(v_{i1}, v_{i2}, v_{i3}, \ldots, v_{id}\right)$, d comprises the dimension of the problem. The best previous particle of the ith particle is recorded and represented as $P_i = \left(p_{i1}, p_{i2}, p_{i3}, \ldots \ldots \ldots \ldots \ldots \ldots \ldots, p_{id}\right)$, the index of the best particle among all the particles is comprised by $P_g = \left(p_{g1} p_{g2} p_{g3} \ldots \ldots \ldots .. p_{gd}\right)$. The velocity and position of each particle can be wangled according to the following equation:

$$V_{id} = \bar{\omega} * V_{id} + \bar{c}_1 * \text{rand} * \left(P_{id} - X_{id}\right) + \bar{c}_2 * \text{rand} * \left(P_{gd} - X_{id}\right) \quad (66)$$

$$X_{id} = X_{id} + V_{id} \quad (67)$$

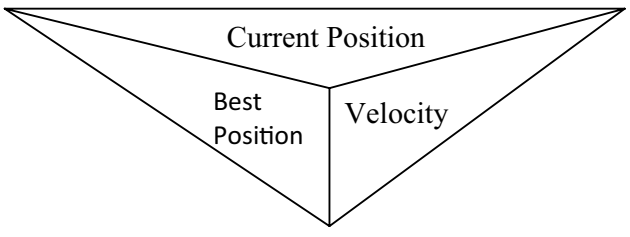

Fig. 11 Schematic structure of a particle in PSO (Kalatehjari 2013)

whereas $\bar{c}_1$ and $\bar{c}_2$ are position constants known as acceleration coefficient, $\bar{\omega}$ is the inertia weight coefficient; rand is a random number within the range [0, 1]. In the present analysis $\bar{\omega}$ is characterized by $\bar{\omega}(\text{gn}) = \bar{\omega}_{\max} - \frac{\bar{\omega}_{\max} - \bar{\omega}_{\min}}{NI} * \text{gn}$, where gn is the generation.

6 PSO Application in Geotechnical Engineering

Complexity of analysis of geotechnical behavior is due to multivariable dependencies of soil and rock responses. Most of the materials that geotechnical engineers deal with show uncertain behavior in consequence of the complex formation of these materials. Therefore, in some geotechnical engineering problems, the objective function is non-convex and discontinuous. Consequently, simple optimization techniques may have difficulties in finding the global optimum solution due to getting trapped in local solutions. To overcome this limitation, using a powerful optimization method to obtain the global optimum solution is of interest. In recent years, soft computing techniques have been widely used to predict geotechnical parameters (Singh et al. 2017; Sharma and Singh 2017). Accordingly, as a powerful optimization technique, PSO has entered in the field of geotechnical engineering to solve its problems. Keeping in view of the feasibility of PSO, in the present analysis PSO is applied to optimize the bearing capacity coefficient.

7 Results and Discussion

Subsequently optimization of bearing capacity coefficient $(N_{\gamma''})$ w.r.t. variables $\alpha_{A1}, \alpha_{A2}, \alpha_{p1}\alpha_{p2}, t/T$ by particle swarm optimization algorithm, optimum $\left(N_{\gamma''}\right)$ can be determined. Minimum value is taken as optimized value. The bearing capacity ratio $\frac{N_{\gamma E}}{N_{\gamma S}}$ is presented in Tables 3, 4, 5, and 6. Ranges of various parameters are given in below:

$$\xi = 10\%, \quad 20\% \ \frac{D_f}{B_0} = 0.25, 0.5, 1 \quad \frac{\phi_1}{\phi_2} = 0.6, 0.8, 1 \quad \frac{\delta_1}{\delta_2} = 0.6, 0.8, 1$$
$$\frac{\gamma_1}{\gamma_2} = 0.6, 0.8, 1 \quad \frac{c_1}{c_2} = 0.6, 0.8, 1 \quad \frac{h_1}{B_0} = 0.25, 0.5, 1 \quad k_v = 0, \frac{k_h}{2}, k_h$$
$$h_1/\lambda, h_2/\lambda = 0.3 \quad h_1/\eta, h_2/\eta = 0.16 \quad \xi_1/\xi_2 = 0.6,\ 0.8,\ 1 \quad \frac{v_{s1}}{v_{s2}} = 0.8 \ \frac{v_{p1}}{v_{p2}} = 0.8$$

where $\lambda = Tv_{s1}$, Tv_{s2} and $\eta = Tv_{p1}$, Tv_{p2}

The parametric study is done for the variation of seismic bearing capacity coefficients with the different soil parameters as shown in Figs. 12, 13, 14, 15, 16, 17, 18, 19 and 20.

i. Variations of seismic bearing capacity coefficient for different values of ξ_1/ξ_2 using particle swarm optimization algorithm:

Table 3 Static bearing capacity coefficients $N_{\gamma S}$ minimum

$\frac{2c_2}{\gamma_2 B_0}=0,\ \frac{c_1}{c_2}=0,\ k_h,k_v=0,\ \xi=10\%$																
ϕ_2	ϕ_1	ϕ_1/ϕ_2	δ_2	δ_1	δ_1/δ_2	γ_1/γ_2	k_v	$k_h=0$								
								$h_1/B_0=0.1$			$h_1/B_0=.25$			$h_1/B_0=.50$		
								d_f/B_0			d_f/B_0			d_f/B_0		
								0.25	0.50	1	0.25	0.50	1	0.25	0.50	1
20	16	0.8	10	8	0.8	0.8	0	6.36	8.85	14.44	5.29	7.03	11.88	4.45	6.95	11.51
							$k_h/2$	6.36	8.85	14.44	5.29	7.03	11.88	4.45	6.95	11.51
							k_h	6.36	8.85	14.44	5.29	7.03	11.88	4.45	6.95	11.51
				10	1	1	0	6.56	9.50	15.22	5.65	8.09	13.39	4.78	7.24	12.33
							$k_h/2$	6.56	9.50	15.22	5.65	8.09	13.39	4.78	7.24	12.33
							k_h	6.56	9.50	15.22	5.65	8.09	13.39	4.78	7.24	12.33
	20	1	20	16	0.8	0.8	0	8.59	12.76	19.90	7.87	11.09	17.56	7.72	10.73	17.00
							$k_h/2$	8.59	12.76	19.90	7.87	11.09	17.56	7.72	10.73	17.00
							k_h	8.59	12.76	19.90	7.87	11.09	17.56	7.72	10.73	17.00
				20	1	1	0	9.22	14.18	22.28	8.12	12.08	20.59	7.61	11.82	19.47
							$k_h/2$	9.22	14.18	22.28	8.12	12.08	20.59	7.61	11.82	19.47
							k_h	9.22	14.18	22.28	8.12	12.08	20.59	7.61	11.82	19.47
25	20	0.8	12.5	10	0.8	0.8	0	11.29	15.70	23.63	9.43	13.69	21.57	8.00	11.76	17.86
							$k_h/2$	11.29	15.70	23.63	9.43	13.69	21.57	8.00	11.76	17.86
							k_h	11.29	15.70	23.63	9.43	13.69	21.57	8.00	11.76	17.86
				12.5	1	1	0	12.30	17.73	27.23	9.83	14.12	23.34	8.21	12.63	19.98
							$k_h/2$	12.30	17.73	27.23	9.83	14.12	23.34	8.21	12.63	19.98
							k_h	12.30	17.73	27.23	9.83	14.12	23.34	8.21	12.63	19.98
	25	1	25	20	0.8	0.8	0	18.94	26.95	39.09	16.78	23.78	37.20	14.16	22.08	34.80
							$k_h/2$	18.94	26.95	39.09	16.78	23.78	37.20	14.16	22.08	34.80
							k_h	18.94	26.95	39.09	16.78	23.78	37.20	14.16	22.08	34.80
				25	1	1	0	20.61	29.88	44.85	17.43	27.92	41.01	16.46	24.28	39.59
							$k_h/2$	20.61	29.88	44.85	17.43	27.92	41.01	16.46	24.28	39.59
							k_h	20.61	29.88	44.85	17.43	27.92	41.01	16.46	24.28	39.59
30	24	0.8	15	12	0.8	0.8	0	22.62	29.89	44.24	18.89	24.30	38.16	17.30	20.35	30.06
							$k_h/2$	22.62	29.89	44.24	18.89	24.30	38.16	17.30	20.35	30.06
							k_h	22.62	29.89	44.24	18.89	24.30	38.16	17.30	20.35	30.06
				15	1	1	0	24.99	32.55	51.43	18.98	26.66	40.23	15.55	21.19	34.68
							$k_h/2$	24.99	32.55	51.43	18.98	26.66	40.23	15.55	21.19	34.68
							k_h	24.99	32.55	51.43	18.98	26.66	40.23	15.55	21.19	34.68
	30	1	30	24	0.8	0.8	0	48.95	62.19	92.25	43.26	58.06	86.15	38.04	50.57	77.20
							$k_h/2$	48.95	62.19	92.25	43.26	58.06	86.15	38.04	50.57	77.20
							k_h	48.95	62.19	92.25	43.26	58.06	86.15	38.04	50.57	77.20
				30	1	1	0	49.65	68.84	103.5	44.82	60.55	97.11	39.65	57.52	89.51
							$k_h/2$	49.65	68.84	103.5	44.82	60.55	97.11	39.65	57.52	89.51
							k_h	49.65	68.84	103.5	44.82	60.55	97.11	39.65	57.52	89.51

Figure 12 depicts the variation of seismic bearing capacity coefficient $(N_{\gamma E})$ with k_h at $\phi_2=30°$, $\delta_2=\frac{\phi_2}{2}$, $\frac{\phi_1}{\phi_2}=0.8$, $\frac{\delta_1}{\delta_2}=0.8$, $\frac{D_f}{B_0}=0.5$, $\xi_2=20\%$, $k_v=\frac{k_h}{2}$, $\frac{\gamma_1}{\gamma_2}=0.8$, $\frac{h_1}{B_0}=0.50$, $\frac{2c_2}{\gamma_2 B_0}=0$, $\frac{c_1}{c_2}=0$, $\frac{v_{s1}}{v_{s2}}=0.8$ h_1/λ, $h_2/\lambda=0.3$, h_1/η, $h_2/\eta=0.16$, $\frac{v_{p1}}{v_{p2}}=0.8$. From this plot, it is seen that coefficient $N_{\gamma E}$ increases with the increase in the value of ξ_1/ξ_2. It is also obvious as increase in damping properties of soil increases the resistance of the soil grains below the foundation and thus increases the bearing capacity.

Table 4 Seismic and static bearing capacity coefficients ratio $\frac{N_{\gamma E}}{N_{\gamma S}}$ minimum

$\frac{2c_2}{\gamma_2 B_0}=0,\ \frac{c_1}{c_2}=0,\ \xi=10\%$															
ϕ_2	ϕ_1/ϕ_2	δ_2	δ_1	δ_1/δ_2	γ_1/γ_2	k_v	$k_h=0.1$								
							$h_1/B_0=0.1$			$h_1/B_0=0.25$			$h_1/B_0=0.50$		
							D_f/B_0			D_f/B_0			D_f/B_0		
							0.25	0.50	1	0.25	0.50	1	0.25	0.50	1
20	0.8	10	8	0.8	0.8	0	0.743	0.799	0.624	0.821	0.749	0.705	0.822	0.715	0.640
						$k_h/2$	0.664	0.611	0.594	0.597	0.721	0.665	0.565	0.638	0.617
						k_h	0.550	0.608	0.583	0.577	0.577	0.665	0.550	0.567	0.587
			10	1	1	0	0.755	0.782	0.628	0.867	0.783	0.709	0.785	0.830	0.694
						$k_h/2$	0.637	0.716	0.616	0.716	0.773	0.653	0.693	0.706	0.654
						k_h	0.596	0.696	0.593	0.586	0.764	0.612	0.528	0.612	0.607
	1	20	16	0.8	0.8	0	0.751	0.755	0.708	0.816	0.751	0.735	0.730	0.718	0.733
						$k_h/2$	0.712	0.648	0.698	0.767	0.676	0.729	0.556	0.676	0.704
						k_h	0.676	0.613	0.665	0.718	0.662	0.696	0.522	0.649	0.666
			20	1	1	0	0.792	0.706	0.704	0.868	0.732	0.727	0.906	0.627	0.754
						$k_h/2$	0.755	0.615	0.697	0.838	0.692	0.710	0.855	0.597	0.710
						k_h	0.686	0.573	0.674	0.725	0.658	0.686	0.688	0.590	0.607
25	0.8	12.5	10	0.8	0.8	0	0.623	0.621	0.684	0.702	0.669	0.741	0.760	0.735	0.816
						$k_h/2$	0.576	0.606	0.638	0.698	0.614	0.689	0.712	0.652	0.702
						k_h	0.555	0.576	0.618	0.660	0.598	0.679	0.680	0.569	0.662
			12.5	1	1	0	0.637	0.594	0.683	0.710	0.693	0.789	0.825	0.772	0.773
						$k_h/2$	0.591	0.540	0.676	0.657	0.626	0.777	0.614	0.622	0.710
						k_h	0.590	0.535	0.667	0.654	0.607	0.743	0.534	0.554	0.689
	1	25	20	0.8	0.8	0	0.532	0.556	0.680	0.517	0.612	0.685	0.607	0.639	0.705
						$k_h/2$	0.492	0.539	0.666	0.515	0.550	0.680	0.481	0.583	0.700
						k_h	0.474	0.498	0.643	0.504	0.530	0.657	0.466	0.518	0.661
			25	1	1	0	0.712	0.706	0.694	0.804	0.691	0.714	0.793	0.741	0.717
						$k_h/2$	0.637	0.671	0.642	0.747	0.684	0.690	0.701	0.689	0.695
						k_h	0.496	0.558	0.621	0.586	0.590	0.641	0.515	0.573	0.662
30	0.8	15	12	0.8	0.8	0	0.575	0.671	0.640	0.630	0.721	0.738	0.686	0.761	0.769
						$k_h/2$	0.560	0.615	0.602	0.587	0.708	0.680	0.647	0.748	0.729
						k_h	0.534	0.595	0.594	0.574	0.671	0.653	0.589	0.706	0.687
			15	1	1	0	0.640	0.619	0.641	0.733	0.719	0.755	0.718	0.809	0.773
						$k_h/2$	0.599	0.572	0.599	0.616	0.690	0.691	0.712	0.714	0.786
						k_h	0.591	0.549	0.592	0.596	0.640	0.680	0.658	0.648	0.695
	1	30	24	0.8	0.8	0	0.617	0.637	0.678	0.666	0.585	0.712	0.754	0.638	0.744
						$k_h/2$	0.595	0.634	0.665	0.644	0.568	0.681	0.696	0.621	0.717
						k_h	0.564	0.604	0.662	0.579	0.538	0.612	0.611	0.574	0.653
			30	1	1	0	0.805	0.729	0.694	0.856	0.806	0.682	0.963	0.769	0.712
						$k_h/2$	0.787	0.724	0.647	0.832	0.748	0.652	0.945	0.686	0.691
						k_h	0.630	0.632	0.600	0.621	0.589	0.648	0.692	0.584	0.680

ii. Variations of seismic bearing capacity coefficient for different values of $\frac{D_f}{B_0}$ using particle swarm optimization algorithm:

Figure 13 depicts the variations of seismic bearing capacity coefficient $(N_{\gamma E})$ with k_h at $\phi_2 = 30^0$, $\delta_2 = \frac{\phi_2}{2}$, $\frac{\phi_1}{\phi_2} = 0.8$, $\frac{\delta_1}{\delta_2} = 0.8$, $k_v = \frac{k_h}{2}$, $\frac{\gamma_1}{\gamma_2} = 0.8$, $\frac{h_1}{B_0} = 0.50$, $\frac{2c_2}{\gamma_2 B_0} = 0.2$, $\frac{c_1}{c_2} = 0$, $\xi_2 = 20\%$, $\xi_1/\xi_2 = 0.8$, $\frac{v_{s1}}{v_{s2}} = 0.8$, h_1/λ, $h_2/\lambda = 0.3, h_1/\eta$, h_2/η=0.16, $\frac{v_{p1}}{v_{p2}} = 0.8$. From this plot, it is seen that coefficient $N_{\gamma E}$ increases with the increase in the value of $\frac{D_f}{B_0}$. It is also obvious as increase

Table 5 Static bearing capacity coefficients $N_{\gamma S}$ minimum

$\frac{2c_2}{\gamma_2 B_0} = 0.20,\ k_h, k_v = 0,\ \xi = 10\%$															
ϕ_2	ϕ_1/ϕ_2	δ_2	c_1/c_2	δ_1/δ_2	γ_1/γ_2	k_v	$k_h=0, k_v=0$								
							$h_1/B_0=0.1$			$h_1/B_0=0.25$			$h_1/B_0=0.50$		
							D_f/B_0			D_f/B_0			D_f/B_0		
							0.25	0.5	1	0.25	0.5	1	0.25	0.5	1
20	0.8	10	0.8	0.8	0.8	0	9.25	11.83	15.69	9.09	9.90	14.89	7.40	9.52	13.03
						$k_h/2$	9.25	11.83	15.69	9.09	9.90	14.89	7.40	9.52	13.03
						k_h	9.25	11.83	15.69	9.09	9.90	14.89	7.40	9.52	13.03
			1	1	1	0	9.32	12.24	17.42	7.98	10.19	15.05	7.08	9.57	13.36
						$k_h/2$	9.32	12.24	17.42	7.98	10.19	15.05	7.08	9.57	13.36
						k_h	9.32	12.24	17.42	7.98	10.19	15.05	7.08	9.57	13.36
	1	20	0.8	0.8	0.8	0	12.83	16.36	22.21	10.93	14.67	21.72	10.76	14.54	21.15
						$k_h/2$	12.83	16.36	22.21	10.93	14.67	21.72	10.76	14.54	21.15
						k_h	12.83	16.36	22.21	10.93	14.67	21.72	10.76	14.54	21.15
			1	1	1	0	12.74	17.20	25.86	11.43	16.37	24.29	11.72	15.74	23.99
						$k_h/2$	12.74	17.20	25.86	11.43	16.37	24.29	11.72	15.74	23.99
						k_h	12.74	17.20	25.86	11.43	16.37	24.29	11.72	15.74	23.99
25	0.8	12.5	0.8	0.8	0.8	0	15.36	18.65	26.72	12.69	16.50	23.96	12.03	14.28	21.71
						$k_h/2$	15.36	18.65	26.72	12.69	16.50	23.96	12.03	14.28	21.71
						k_h	15.36	18.65	26.72	12.69	16.50	23.96	12.03	14.28	21.71
			1	1	1	0	15.88	20.77	29.87	12.77	17.06	24.67	11.32	14.94	22.85
						$k_h/2$	15.88	20.77	29.87	12.77	17.06	24.67	11.32	14.94	22.85
						k_h	15.88	20.77	29.87	12.77	17.06	24.67	11.32	14.94	22.85
	1	25	0.8	0.8	0.8	0	24.05	33.09	49.50	21.34	29.25	44.60	21.10	29.71	42.94
						$k_h/2$	24.05	33.09	49.50	21.34	29.25	44.60	21.10	29.71	42.94
						k_h	24.05	33.09	49.50	21.34	29.25	44.60	21.10	29.71	42.94
			1	1	1	0	28.73	36.82	55.40	26.65	35.72	55.14	25.29	34.68	48.55
						$k_h/2$	28.73	36.82	55.40	26.65	35.72	55.14	25.29	34.68	48.55
						k_h	28.73	36.82	55.40	26.65	35.72	55.14	25.29	34.68	48.55
30	0.8	15	0.8	0.8	0.8	0	28.41	35.88	46.45	24.39	31.95	41.68	22.59	26.82	38.98
						$k_h/2$	28.41	35.88	46.45	24.39	31.95	41.68	22.59	26.82	38.98
						k_h	28.41	35.88	46.45	24.39	31.95	41.68	22.59	26.82	38.98
			1	1	1	0	29.65	37.09	52.94	24.55	31.82	45.87	22.04	28.07	40.50
						$k_h/2$	29.65	37.09	52.94	24.55	31.82	45.87	22.04	28.07	40.50
						k_h	29.65	37.09	52.94	24.55	31.82	45.87	22.04	28.07	40.50
	1	30	0.8	0.8	0.8	0	60.94	82.54	115.0	57.39	71.44	111.7	54.10	70.35	100.6
						$k_h/2$	60.94	82.54	115.0	57.39	71.44	111.7	54.10	70.35	100.6
						k_h	60.94	82.54	115.0	57.39	71.44	111.7	54.10	70.35	100.6
			1	1	1	0	80.94	101.1	131.0	73.08	89.04	128.1	68.31	88.67	114.0
						$k_h/2$	80.94	101.1	131.0	73.08	89.04	128.1	68.31	88.67	114.0
						k_h	80.94	101.1	131.0	73.08	89.04	128.1	68.31	88.67	114.0

in depth increases the confinement of the soil grains below the foundation. Thus, by increasing $\frac{D_f}{B_0}$ bearing capacity of the foundation increases.

iii. Variations of seismic bearing capacity coefficient for different values of k_v using particle swarm optimization algorithm:

Figure 14 shows the variations of $(N_{\gamma E})$ with k_h at $\phi_2 = 30°$, $\delta_2 = \frac{\phi_2}{2}$, $\frac{h_1}{B_0} = 0.50$, $\frac{\gamma_1}{\gamma_2} = 0.8$, $\frac{\delta_1}{\delta_2} = 0.8$,

Table 6 Seismic and static bearing capacity coefficients $\frac{N_{\gamma E}}{N_{\gamma S}}$ minimum

ϕ_2	ϕ_1/ϕ_2	δ_2	c_1/c_2	δ_1/δ_2	γ_1/γ_2	k_v	$k_h=0.1$								
							$h_1/B_0=0.1$			$h_1/B_0=0.25$			$h_1/B_0=0.50$		
							D_f/B_0			D_f/B_0			D_f/B_0		
							0.25	0.5	1	0.25	0.5	1	0.25	0.5	1
20	0.8	10	0.8	0.8	0.8	0	--	0.690	0.734	0.632	0.790	0.704	0.606	0.752	0.737
						$k_h/2$	0.620	0.629	0.666	0.593	0.732	0.689	0.543	0.630	0.672
						k_h	0.565	0.578	0.633	0.566	0.657	0.613	0.426	0.546	0.643
			1	1	1	0	0.715	0.761	0.785	0.776	0.857	0.794	0.642	0.721	0.870
						$k_h/2$	0.692	0.678	0.758	0.738	0.798	0.765	0.637	0.661	0.849
						k_h	0.657	0.657	0.697	0.655	0.721	0.684	0.628	0.528	0.752
	1	20	0.8	0.8	0.8	0	0.636	0.670	0.720	0.735	0.676	0.727	0.660	0.610	0.706
						$k_h/2$	0.596	0.634	0.701	0.695	0.627	0.695	0.594	0.568	0.689
						k_h	0.531	0.609	0.695	0.591	0.613	0.662	0.578	0.555	0.668
			1	1	1	0	0.654	0.733	0.675	0.712	0.754	0.716	0.676	0.735	0.683
						$k_h/2$	0.639	0.657	0.660	0.692	0.682	0.698	0.623	0.676	0.677
						k_h	0.635	0.647	0.650	0.648	0.647	0.660	0.606	0.627	0.635
25	0.8	12.5	0.8	0.8	0.8	0	0.698	0.740	0.757	0.754	0.734	0.767	0.727	0.848	0.775
						$k_h/2$	0.640	0.703	0.753	0.727	0.709	0.752	0.634	0.747	0.750
						k_h	0.591	0.650	0.677	0.632	0.651	0.714	0.565	0.690	0.735
			1	1	1	0	0.672	0.714	0.715	0.816	0.749	0.759	0.808	0.784	0.717
						$k_h/2$	0.617	0.667	0.670	0.751	0.709	0.748	0.602	0.740	0.704
						k_h	0.574	0.650	0.666	0.684	0.656	0.737	0.592	0.698	0.662
	1	25	0.8	0.8	0.8	0	0.634	0.758	0.576	0.701	0.757	0.607	0.613	0.606	0.515
						$k_h/2$	0.631	0.699	0.565	0.595	0.654	0.566	0.555	0.555	0.493
						k_h	0.610	0.624	0.533	0.539	0.601	0.550	0.438	0.458	0.469
			1	1	1	0	0.580	0.612	0.629	0.573	0.577	0.573	0.485	0.559	0.641
						$k_h/2$	0.579	0.556	0.591	0.572	0.502	0.562	0.452	0.517	0.632
						k_h	0.492	0.516	0.582	0.529	0.453	0.548	0.410	0.499	0.620
30	0.8	15	0.8	0.8	0.8	0	0.695	0.671	0.756	0.750	0.740	0.760	0.633	0.688	0.638
						$k_h/2$	0.682	0.622	0.736	0.662	0.693	0.672	0.567	0.622	0.631
						k_h	0.577	0.615	0.713	0.578	0.525	0.659	0.533	0.549	0.592
			1	1	1	0	0.666	0.740	0.742	0.690	0.708	0.763	0.736	0.716	0.785
						$k_h/2$	0.620	0.692	0.702	0.666	0.687	0.747	0.699	0.666	0.669
						k_h	0.559	0.626	0.689	0.626	0.604	0.700	0.588	0.601	0.691
	1	30	0.8	0.8	0.8	0	0.707	0.694	0.610	0.726	0.727	0.597	0.774	0.700	0.598
						$k_h/2$	0.647	0.655	0.586	0.720	0.632	0.566	0.695	0.651	0.586
						k_h	0.633	0.591	0.562	0.617	0.554	0.557	0.607	0.476	0.584
			1	1	1	0	0.530	0.544	0.700	0.557	0.598	0.699	0.545	0.541	0.761
						$k_h/2$	0.525	0.540	0.699	0.545	0.574	0.696	0.542	0.510	0.760
						k_h	0.506	0.539	0.692	0.518	0.547	0.691	0.480	0.510	0.690

UB upper bound, *LB* lower bound

$\frac{\phi_1}{\phi_2}=0.8$, $\frac{D_f}{B_0}=0.5$, $\frac{2c_2}{\gamma_2 B_0}=0.2$, $\frac{c_1}{c_2}=0$, $\xi=20\%$, $\xi_1/\xi_2=0.8$, $\frac{v_{s1}}{v_{s2}}=0.8$, h_1/λ, $h_2/\lambda=0.3$, h_1/η, h_2/η=0.16, $\frac{v_{p1}}{v_{p2}}=0.8$. From the plot, it is seen that $N_{\gamma E}$ decreases with the increase in the value of k_v. It is obvious because increase in the value of k_v will increase the disturbance of base soil, and this result decreases the value of $N_{\gamma E}$.

iv. Variations of seismic bearing capacity coefficient for different values of $\frac{\delta_1}{\delta_2}$ using particle swarm optimization algorithm:

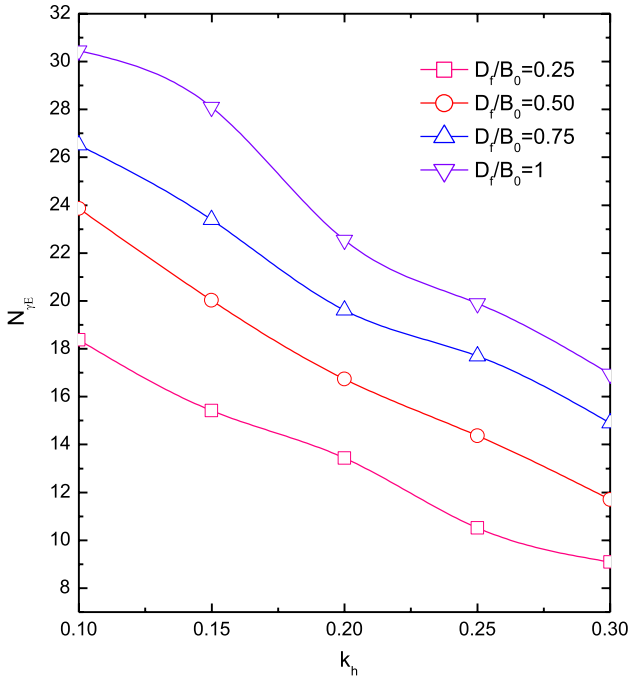

Fig. 12 Variation of $N_{\gamma E}$ with k_{h} for $\phi_2 = 30°$, $\delta_2 = \phi_2/2$, $\phi_1/\phi_2 = 0.8$, $\delta_1/\delta_2 = 0.8$, $k_V = k_h/2$, $\gamma_1/\gamma_2 = 0.8$, $h_1/B_0 = 0.25$ $2c_2/B_0\gamma_2 = 0.2$, c_1/c_2=0.8, h_1/λ, h_2/λ=0.3, h_1/η, h_2/η=0.16, $V_{\mathrm{S1}}/V_{\mathrm{S2}}$, $V_{\mathrm{p1}}/V_{\mathrm{p2}}$=0.8

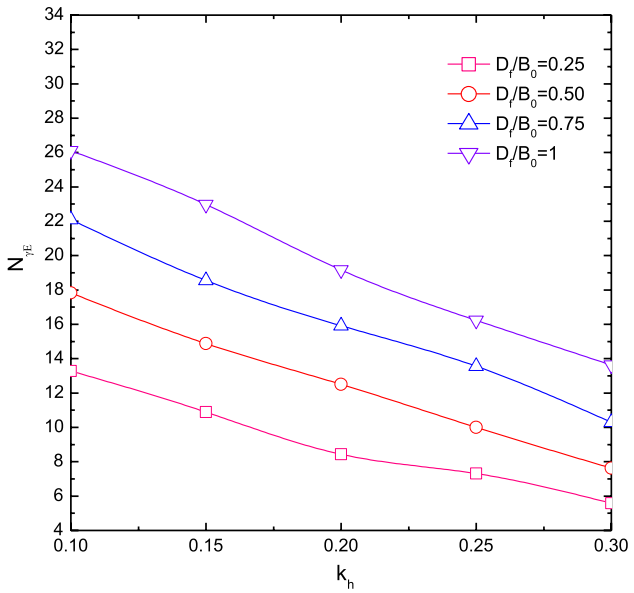

Fig. 13 Variation of $N_{\gamma E}$ with k_{h} for $\phi_2 = 30°$, $\delta_2 = \phi_2/2$, $\xi_2 = 20\%$ $h_1/B_0 = 0.50$, $\phi_1/\phi_2 = 0.8$, $\delta_1/\delta_2 = 0.8$, $k_V = k_h/2$, $\gamma_1/\gamma_2 = 0.8$, $\xi_1/\xi_2 = 0.8$, $2c_2/B_0\gamma_2 = 0.2$, c_1/c_2=0, h_1/λ, h_2/λ=0.3, h_1/η, h_2/η=0.16, $V_{\mathrm{S1}}/V_{\mathrm{S2}}$, $V_{\mathrm{p1}}/V_{\mathrm{p2}}$=0.8

Figure 15 shows the variations of seismic bearing capacity coefficient $(N_{\gamma E})$ with k_h at $\phi_2 = 30°$, $\delta_2 = \frac{\phi_2}{2}$,

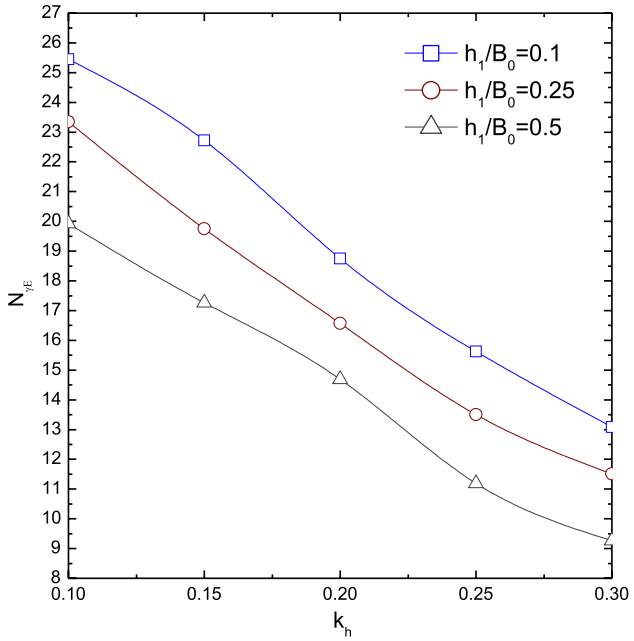

Fig. 14 Variation of $N_{\gamma E}$ with k_{h} for $\phi_2 = 30°$, $\delta_2 = \phi_2/2$, $\phi_1/\phi_2 = 0.8$, $\delta_1/\delta_2 = 0.8$, $k_V = k_h/2$, $\gamma_1/\gamma_2 = 0.8$, D_{f}/B_0=0.50, $2c_2/B_0\gamma_2 = 0.2$, c_1/c_2=0.8 h_1/γ, h_2/γ=0.3, h_1/η, h_2/η=0.16, $V_{\mathrm{S1}}/V_{\mathrm{S2}}$, $V_{\mathrm{p1}}/V_{\mathrm{p2}}$=0.8

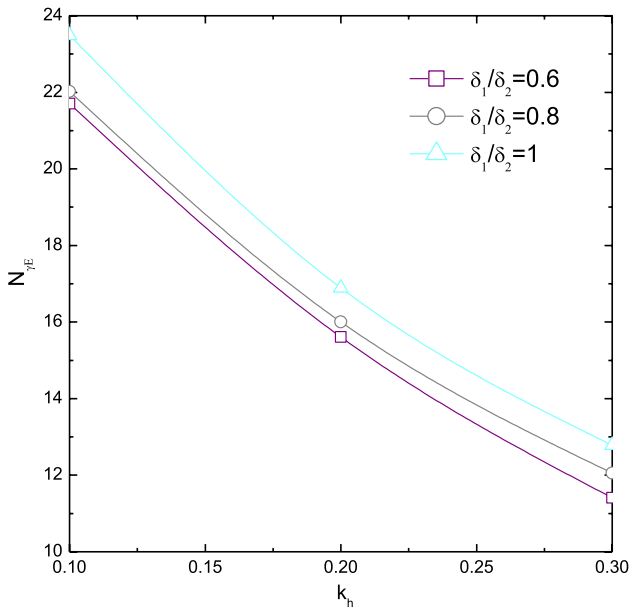

Fig. 15 Variation of $N_{\gamma E}$ with k_{h} for $\phi_2 = 30°$, $\delta_2 = \phi_2/2$, $\phi_1/\phi_2 = 0.8$, D_{f}/B_0=0.8, $k_V = k_h/2$, $h_1/B_2 = 0.25$, $2c_2/B_0\gamma_2 = 0.2$, c_1/c_2=0.8 h_1/γ, h_2/γ=0.3, h_1/η, h_2/η=0.16, $V_{\mathrm{S1}}/V_{\mathrm{S2}}$, $V_{\mathrm{p1}}/V_{\mathrm{p2}}$=0.8

$\frac{\mathrm{h_1}}{B_0} = 0.5$, $\frac{\gamma_1}{\gamma_2} = 0.8$, $k_v = \frac{k_h}{2}$, $\frac{\phi_1}{\phi_2} = 0.8$, $\frac{D_{\mathrm{f}}}{B_0} = 0.5$, $\frac{2c_2}{\gamma_2 B_0} = 0$, $\frac{c_1}{c_2} = 0$, $\xi = 20\%$, $\xi_1/\xi_2 = 0.8$, $\frac{v_{s1}}{v_{s2}} = 0.8$, h_1/λ, $h_2/\lambda = 0.3, h_1/\eta$, h_2/η=0.16, $\frac{v_{p1}}{v_{\mathrm{p2}}} = 0.8$. From the

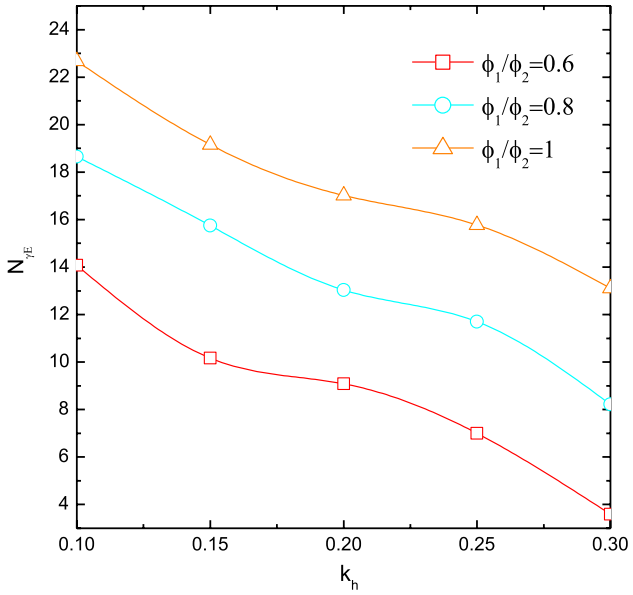

Fig. 16 Variation of $N_{\gamma E}$ with k_h for $\phi_2 = 30°$, $\delta_2 = \phi_2/2$, $\xi_2 = 20\%$, $h_1/B_0 = 0.50$ δ_1/δ_2=0.8, k_v=k_h/2, ξ_1/ξ_2=0.8, $\gamma_1/\gamma_2 = 0.8$, D_f/B_0=0.50, $2c_2/B_0\ \gamma_2 = 0$, c_1/c_2=0 h_1/γ, h_2/γ=0.3, h_1/η, h_2/η=0.16, V_{S1}/V_{S2}=0.8, V_{p1}/V_{p2}=0.8

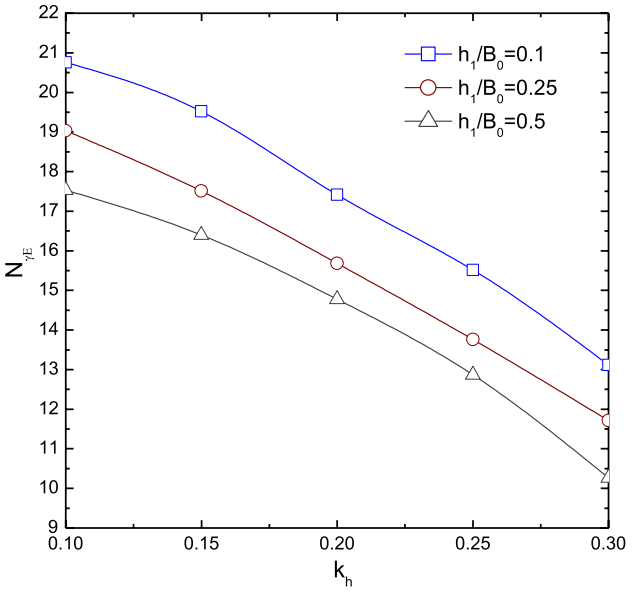

Fig. 18 Variation of $N_{\gamma E}$ with k_h for $\phi_2 = 30°$, $\delta_2 = \phi_2/2$, $\xi_2 = 20\%$, $\gamma_1/\gamma_2 = 0.8$ δ_1/δ_2=0.8, k_v=k_h/2, ξ_1/ξ_2=0.8, $\phi_1/\phi_2 = 0.8$, D_f/B_0=0.50, $2c_2/B_0\ \gamma_2 = 0$, c_1/c_2=0 h_1/γ, h_2/γ=0.3, h_1/η, h_2/η=0.16, V_{S1}/V_{S2}=0.8, V_{p1}/V_{p2}=0.8

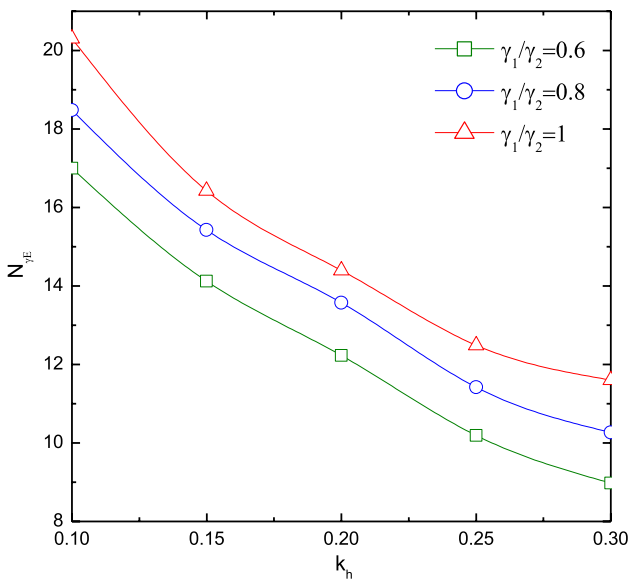

Fig. 17 Variation of $N_{\gamma E}$ with k_h for $\phi_2 = 30°$, $\delta_2 = \phi_2/2$, $\xi_2 = 20\%$, $h_1/B_0 = 0.50$ δ_1/δ_2=0.8, k_v=k_h/2, ξ_1/ξ_2=0.8, $\phi_1/\phi_2 = 0.8$, D_f/B_0=0.50, $2c_2/B_0\ \gamma_2 = 0$, c_1/c_2=0 h_1/γ, h_2/γ=0.3, h_1/η, h_2/η=0.16, V_{S1}/V_{S2}=0.8, V_{p1}/V_{p2}=0.8

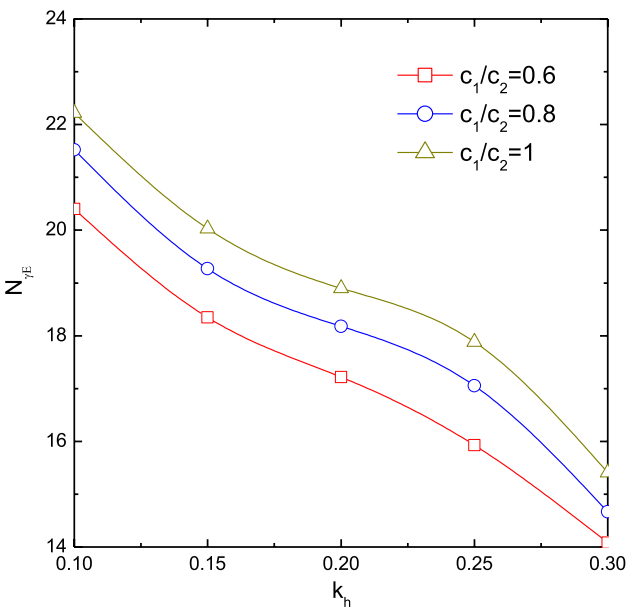

Fig. 19 Variation of $N_{\gamma E}$ with k_h for $\phi_2 = 30°$, $\delta_2 = \phi_2/2$, $\xi_2 = 20\%$, h_1/B_0=0.50 δ_1/δ_2=0.8, k_v=k_h/2, ξ_1/ξ_2=0.8, $\phi_1/\phi_2 = 0.8$, D_f/B_0=0.50, $2c_2/B_0\ \gamma_2 = 0.2$, h_1/γ, h_2/γ=0.3, h_1/η, h_2/η=0.16, V_{S1}/V_{S2}=0.8, V_{p1}/V_{p2}=0.8

plot, it is seen that coefficient $N_{\gamma E}$ increases with the increase in the value of $\frac{\delta_1}{\delta_2}$. Here, increase in δ_1 value is made keeping the δ_2 value as a constant. So, obviously due to the increase in $\frac{\delta_1}{\delta_2}$ ratio, the value $N_{\gamma E}$ will increase

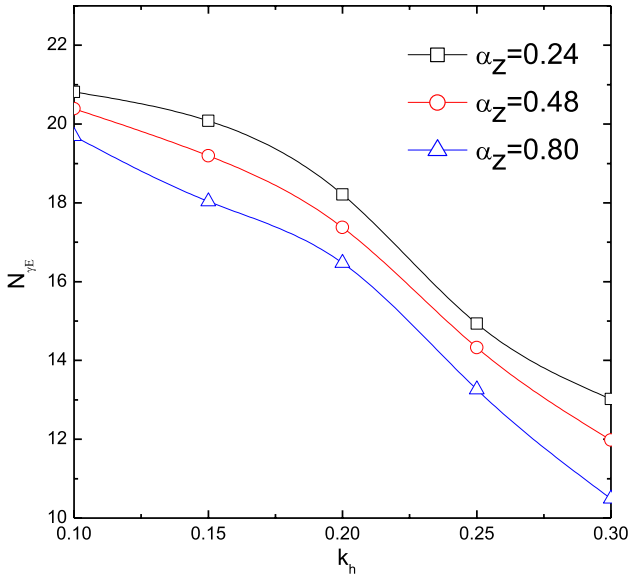

Fig. 20 Variation of $N_{\gamma E}$ with k_h for $\phi_2 = 30°$, $\delta_2 = \phi_2/2$, $\xi_2 = 20\%$, $h_1/B_0 = 0.50$ $\delta_1/\delta_2 = 0.8$, $k_v = k_h/2$, $\xi_1/\xi_2 = 0.8$, $\phi_1/\phi_2 = 0.8$ $D_f/B_0 = 0.50$, $2c_2/B_0\,\gamma_2 = 0$, $c_1/c_2 = 0$ h_1/γ, $h_2/\gamma = 0.3$, h_1/η, $h_2/\eta = 0.16$

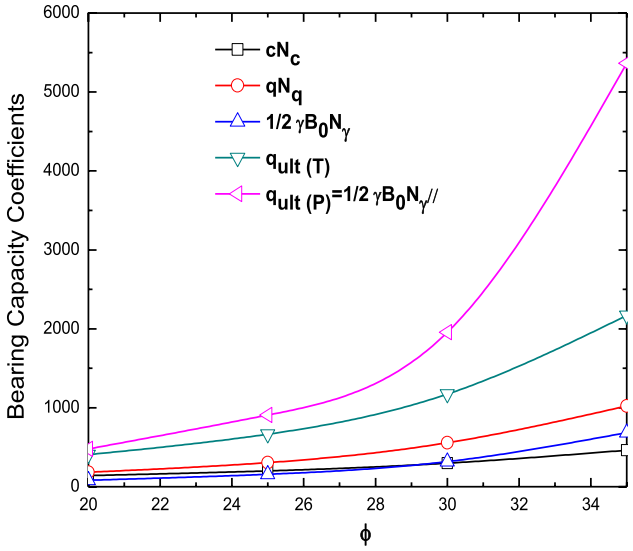

Fig. 21 Variation of bearing capacity coefficients with ϕ for $\gamma = 19$ kN/m^3, $B_0 = 1.7$ m, $D_f = 1.3$ m, $c = 8$ kN/m^2

v. Variations of seismic bearing capacity coefficient for different values of $\frac{\phi_1}{\phi_2}$ using particle swarm optimization algorithm:

Figure 16 depicts the variations of seismic bearing capacity coefficient $(N_{\gamma E})$ with k_h at $\phi_2 = 30°$, $\delta_2 = \frac{\phi_2}{2}$, $\frac{h_1}{B_0} = 0.50$, $\frac{\delta_1}{\delta_2} = 0.8$, $k_v = \frac{k_h}{2}$, $\frac{\gamma_1}{\gamma_2} = 0.8$, $\frac{D_f}{B_0} = 0.5$, $\frac{2c_2}{\gamma_2 B_0} = 0$, $\frac{c_1}{c_2} = 0$, $\xi = 20\%$, $\xi_1/\xi_2 = 0.8$, $\frac{v_{s1}}{v_{s2}} = 0.8$, h_1/λ, $h_2/\lambda = 0.3, h_1/\eta$, $h_2/\eta = 0.16, \frac{v_{p1}}{v_{p2}} = 0.8$. From the figure, it is seen that coefficient $N_{\gamma E}$ increases with the increase in the value of $\frac{\phi_1}{\phi_2}$. Here increase in ϕ_1 value is made keeping the ϕ_2 value as constant.

vi. Variations of seismic bearing capacity coefficient for different values of $\frac{\gamma_1}{\gamma_2}$ using particle swarm optimization algorithm:

Figure 17 shows the variations of seismic bearing capacity coefficient $(N_{\gamma E})$ with k_h at $\phi_2 = 30°$, $\delta_2 = \frac{\phi_2}{2}$, $\frac{h_1}{B_0} = 0.50$, $\frac{\delta_1}{\delta_2} = 0.8$, $k_v = \frac{k_h}{2}$, $\frac{\phi_1}{\phi_2} = 0.8$, $\frac{D_f}{B_0} = 0.5$, $\frac{2c_2}{\gamma_2 B_0} = 0$, $\frac{c_1}{c_2} = 0$, $\xi = 20\%$, $\xi_1/\xi_2 = 0.8$, $\frac{v_{s1}}{v_{s2}} = 0.8$, h_1/λ, $h_2/\lambda = 0.3, h_1/\eta$, $h_2/\eta = 0.16, \frac{v_{p1}}{v_{p2}} = 0.8$. From the figure, it is seen coefficient $N_{\gamma E}$ increases with the increase in the value of $\frac{\gamma_1}{\gamma_2}$. Here, $\frac{\gamma_1}{\gamma_2}$ ratio is increased keeping γ_2 as constant.

vii. Variations of seismic bearing capacity coefficient for different values of $\frac{h_1}{B_0}$ using particle swarm optimization algorithm:

Figure 18 shows the variations of seismic bearing capacity coefficient $(N_{\gamma E})$ with k_h at $\phi_2 = 30°$, $\delta_2 = \frac{\phi_2}{2}$, $\frac{\phi_1}{\phi_2} = 0.8$, $\frac{\delta_1}{\delta_2} = 0.8$, $k_v = \frac{k_h}{2}$, $\frac{\gamma_1}{\gamma_2} = 0.8$, $\frac{D_f}{B_0} = 0.5$, $\frac{2c_2}{\gamma_2 B_0} = 0$, $\frac{c_1}{c_2} = 0$, $\xi = 20\%$, $\xi_1/\xi_2 = 0.8$, $\frac{v_{s1}}{v_{s2}} = 0.8$, h_1/λ, $h_2/\lambda = 0.3, h_1/\eta$, $h_2/\eta = 0.16, \frac{v_{p1}}{v_{p2}} = 0.8$. From the figure, it is seen that coefficient $N_{\gamma E}$ decreases with the increase in the value of $\frac{h_1}{B_0}$. Here, h_1 is the depth of the top layer and it is considered in the analysis that it is weaker than the bottom layer. So, weaker layer will provide less resistance and hence increase in the thickness of this layer decreases the value of bearing capacity coefficient.

viii. Variations of seismic bearing capacity coefficient for different values of $\frac{c_1}{c_2}$ using particle swarm optimization algorithm:

Figure 19 shows the variations of $(N_{\gamma E})$ with k_h at $\phi_2 = 30°, \delta_2 = \frac{\phi_2}{2}, \frac{h_1}{B_0} = 0.50, \frac{\gamma_1}{\gamma_2} = 0.8, k_v = \frac{k_h}{2}, \frac{\phi_1}{\phi_2} = 0.8$, $\frac{D_f}{B_0} = 0.5$, $\frac{2c_2}{\gamma_2 B_0} = 0.2$, $k_v = \frac{k_h}{2}$, $\xi = 20\%$, $\xi_1/\xi_2 = 0.8$, $\frac{v_{s1}}{v_{s2}} = 0.8, h_1/\lambda$, $h_2/\lambda = 0.3, h_1/\eta$, $h_2/\eta = 0.16, \frac{v_{p1}}{v_{p2}} = 0.8$. From the plot, it is seen that the coefficient $N_{\gamma E}$ increases with the increase in the values $\frac{c_1}{c_2}$. Here, $\frac{c_1}{c_2}$ ratio is increased while keeping c_2 as constant. So, obviously due to the increase in $\frac{c_1}{c_2}$ ratio, the value $N_{\gamma E}$ will increase.

ix. Variations of seismic bearing capacity coefficient for different values of impedance ratio α_z using particle swarm optimization algorithm: variations of seismic bearing capacity coefficient for different values of impedance ratio α_z using particle swarm optimization algorithm:

Figure 20 shows the variations of $(N_{\gamma E})$ at $\phi_2 = 30°$, $\delta_2 = \frac{\phi_2}{2}, \frac{h_1}{B_0} = 0.50, \frac{\gamma_1}{\gamma_2} = 0.8, k_v = \frac{k_h}{2}, \frac{\phi_1}{\phi_2} = 0.8, \frac{D_f}{B_0} = 0.5$,

Table 7 Comparison of $\frac{q_u}{\gamma_1 B_0}$ values in four series with experimental data from Kumar et al. (2007) and Khatri et al. (2017) for rough strip footing on two-layered soil

Test series	h_1/B_0	Khatri et al. (2017)		Kumar et al. (2007)	Present analysis	% of difference		
						Khatri et al. (2017)		Kumar et al. (2007)
		L.B	U.B			L.B	U.B	
1. $\phi_1=35°$, $\phi_2=32°$, $\gamma_1=16.24$ kN/m^3, $\gamma_2=15.05$ kN/m^3	0.5	13.04	13.5	14.14	12.5435	3.80%	7.08%	11.29%
	1	15.99	16.57	14.98	17.3471	− 8.48%	− 4.68%	− 15.76%
	1.5	16.73	17.42	15.46	19.6001	− 17.16%	− 12.52%	− 26.77%
	2	19.54	20.35	16.22	21.1253	− 8.11%	− 3.80%	− 30.24%
2. $\phi_1=37°$, $\phi_2=35°$,$\gamma_1=16.44$ kN/m^3, $\gamma_2=15.15$ kN/m^3	0.5	19.59	20.35	22.47	20.1538	− 2.88%	4.96%	10.30%
	1	22.69	23.63	23.32	23.6043	− 4.03%	0.10%	− 1.22%
	1.5	23.78	24.85	24.33	25.3011	− 6.40%	− 1.82%	− 3.99%
	2	23.75	24.84	25.47	29.7838	− 25.40%	− 19.90%	− 16.90%
3. $\phi_1=39°$, $\phi_2=36°$, $\gamma_1=16.35$ kN/m^3, $\gamma_2=15.25$ kN/m^3	0.5	24.97	26.05	30.17	27.4622	− 9.98%	− 5.42%	8.97%
	1	30.55	31.9	31.62	32.0822	− 5.01%	− 0.57%	− 1.46%
	1.5	34.09	35.87	33.27	33.7438	1.02%	5.93%	− 1.42%
	2	34.01	35.85	34.8	34.8682	− 2.52%	2.73%	− 0.19%
4. $\phi_1=41°$, $\phi_2=37°$, $\gamma_1=16.76$ kN/m^3, $\gamma_2=15.58$ kN/m^3	0.5	31.78	33.24	37.19	29.5145	7.12%	11.20%	20.60%
	1	40.74	42.62	39.26	34.1436	16.20%	19.88%	13.03%
	1.5	48.94	51.12	41.37	39.8574	18.55%	22.03%	3.65%
	2	49.69	52.51	43.24	45.2934	8.84%	13.74%	− 4.74%

Table 8 Comparison of $\frac{q_u}{\gamma_1 B_0}$ values with data from Hanna (1981), Farah (2004) and Khatri et al. (2017) for rough strip footing on two-layered soil

h_1/B_0	Khatri et al. (2017)		Hanna (1981)	Farah (2004)	Present	% of difference			
						Hanna (1981)	Farah (2004)	Khatri et al. (2017)	
	LB	UB						L.B	U.B
0	11.92	12.4	18.79	20.38	16.8246	10.45%	17.44%	− 41.10%	− 35.67%
0.25	19.15	19.93	23.5	25.71	19.4047	17.42%	24.52%	− 1.33%	2.63%
0.5	30.76	32.04	31.16	34.82	24.3199	21.95%	30.15%	20.93%	24.09%
1	54.31	56.54	44.92	50.56	56.962	− 26.80%	− 12.66%	− 4.88%	− 0.75%
1.5	83.16	87.03	67	77.14	94.567	− 41.14%	− 22.59%	− 13.72%	− 8.66%
2	108.33	113.86	89.09	101.35	98.1253	− 10.14%	3.18%	9.42%	13.82%

UB upper bound, *LB* lower bound

$\frac{2c_2}{\gamma_2 B_0}=0.2$, $\frac{c_1}{c_2}=0.8$, $k_v=\frac{k_h}{2}$, $\xi=20\%$, $\xi_1/\xi_2=0.8$, $\frac{v_{s1}}{v_{s2}}=0.8, h_1/\lambda$, $h_2/\lambda=0.3, h_1/\eta$, $h_2/\eta=0.16, \frac{v_{p1}}{v_{p2}}=0.8$ with k_h. From the plot, it is seen that the coefficient $N_{\gamma E}$ decreases with the increase in the values α_z.

x. From Terzaghi (1943) we know ultimate bearing capacity $q_{ult}=cN_c+qN_q+0.5\gamma B_0 N_\gamma$, taking $c=8$ kN/m^2, $\gamma=19$ kN/m^3, $B_0=1.7$ m and $D_f=1.3$ m, the values of cN_c, qN_q and $0.5\gamma B_0 N_\gamma$ are evaluated at different values of ϕ and plotted in Fig. 21. Also, in the present methodology, if we put all values of $h_1=0$, $k_h=k_v=0$, then it will give the bearing capacity ($q_{ult(P)}$) of shallow strip footing resting on single-layered soil under static loading condition, which also is shown in Fig. 21. In the same figure, $q_{ult(T)}$ represents the bearing capacity as obtained using Terzaghi's equation. From the plot, it is seen that the present method calculates the bearing capacity 26% higher value in comparison with Terzaghi (1943).

Table 9 Comparison of $\frac{q_u}{\gamma_1 B_0}$ values with data from Hanna (1981) and Khatri et al. (2017) for rough circular footing on two-layered soil

Khatri et al. (2017)		Hanna (1981)	Present	% of difference		
				Hanna (1981)	Khatri et al. (2017)	
LB	UB				L.B	U.B
16.04	17.18	22.41	16.8246	24.92%	– 4.89%	5.73%
22.05	23.58	24.49	19.4047	20.76%	11.99%	17.70%
34.41	39.5	36.75	24.3199	12.43%	29.32%	38.43%
90.76	95.35	61.23	56.962	6.97%	37.23%	40.26%
109.47	116.32	94.95	94.567	0.40%	13.61%	18.70%
156.73	162.83	141.87	98.1253	30.83%	37.39%	39.73%

UB upper bound, *LB* lower bound

Table 10 Comparison of $\frac{q_u}{\gamma_1 B_0}$ values with data from Lotfizadeh and Kamalian (2016) for strip footing on two-layered sandy soil

h_1/B_0	Lotfizadeh and Kamalian (2016)	Present	% of Difference
0	17.888	18.4569	– 3.00%
0.12	16.789	15.5142	7.50%
0.27	12.112	12.6199	– 4.19%
0.34	9.902	12.0774	– 21.90%
0.46	8.432	11.5849	– 37.30%
0.61	7.811	10.9224	– 39.80%

UB upper bound, *LB* lower bound

8 Comparison

A comparison of bearing capacity coefficient values has made for different friction angles. The comparison is made to demonstrate the accuracy of the present methodology. With known formulation for bearing capacity coefficient $N_{\gamma''}$, a computer programing software 'MATLAB' code has been developed using PSO algorithm, which is able to calculate the ultimate bearing capacity, q_{ult}, for various combinations of soil properties in each layer. Table 7 represents a comparison of the present results with the experimental data from Khatri et al. (2017), Kumar et al. (2007) for the strip footing with four different series of experimental data. Table 8 shows a comparison of the present results with corresponding experimental data from Hanna (1981), Khatri et al. (2017) and Farah (2004) for strip footing with ϕ_1 of 47.7°, γ_1 of 16.33 kN/m^3, ϕ_2 of 34°, γ_2 of 13.78 kN/m^3. It is noteworthy that the values of $\frac{q_u}{\gamma_1 B_0}$ given by Farah (2004) were found to be always greater than those given by Hanna (1981). For $\frac{h_1}{B_0}$ values up to 1.0, the values of N_γ from Hanna(1981), Khatri et al. (2017) and Farah (2004) were found to be closer with the present result. The comparison of the present results with those represented by Hanna (1981) for circular footing is presented in Table 9 with ϕ_1 of 47.7°, γ_1 of 16.33 kN/m^3, ϕ_2 of 34°, γ_2 of 13.78 kN/m^3.The present values of $q_u/\gamma_1 B_0$ of h_1/B_0 of 1 or lesser are found to be closer with the corresponding values from Hanna (1981). Table 10 shows comparison between Lotfizadeh and Kamalian (2016) and present analysis. From Table 10, it is seen that the present value gives higher value than Lotfizadeh and Kamalian (2016). A comparison of analytical solution is done with the present analysis. Table 11 represents the

Table 11 Comparison of Bearing Capacity Coefficient ($N_{\gamma''}$) values with values from Debnath and Ghosh (2018) for strip footing on two-layered soil

ϕ_2	ϕ_1/ϕ_2	δ_2	δ_1/δ_2	γ_1/γ_2	k_v	Debnath and Ghosh (2018)			Present analysis		
						$k_h=0.2$			$k_h=0.2$, $\alpha_z=0.8$, $\xi_1/\xi_2=1$		
						$h_1/B_0=0.25$			$h_1/B_0=0.25$		
						D_f/B_0			D_f/B_0		
						0.25	0.5	1	0.25	0.5	1
30	0.8	15	0.8	0.8	0	7.2915	10.935	17.973	7.1934	10.1739	17.2271
					$k_h/2$	6.271	9.6714	16.637	6.4399	8.1455	16.4676
					k_h	5.61	8.5536	14.767	4.7787	8.1368	15.9157
30	1	30	0.8	0.8	0	12.978	19.508	37.04	13.486	20.6214	34.0547
					$k_h/2$	12.631	17.65	33.081	11.9321	15.9021	31.8695
					k_h	11.031	14.515	29.807	9.3429	13.9049	27.9495

Table 12 Comparison with upper-bound and lower-bound values

Ultimate bearing capacity q_u (kPa)for ($\gamma_1 = 18$ kN/m^3, $\gamma_2 = 15$ kN/m^3)									
h_1/B_0		Eshkevari et al. (2019)				Present analysis			
		$\phi_2 = 27.5$, $\phi_1 = 40$	$\phi_2 = 30$, $\phi_1 = 40$	$\phi_2 = 32.5$, $\phi_1 = 40$	$\phi_2 = 35$, $\phi_1 = 40$	$\phi_2 = 27.5$, $\phi_1 = 40$	$\phi_2 = 30$, $\phi_1 = 40$	$\phi_2 = 32.5$, $\phi_1 = 40$	$\phi_2 = 35$, $\phi_1 = 40$
0.2	L.B	360	510	700	970	393.525	515.75	715.37	969.45
	U.B	400	530	720	1050				
0.3	L.B	400	540	730	1020	433.125	534.10	768.24	1020.94
	U.B	440	560	800	1150				
0.4	L.B	470	560	780	1100	484.605	644.98	804.87	1124.39
	U.B	500	620	870	1200				
0.5	L.B	520	600	800	1200		564.3	838.77	1225.62
	U.B	540	680	910	1260				

comparison between Debnath and Ghosh (2018) and present analysis. Table 12 depicts a comparison between upper and lower bound bearing capacities obtained by Eshkevari et al. (2019) and present analysis. The upper-bound and lower-bound bearing capacities were calculated in a series of analyses where the ratio of thickness of top layer to width of footing (h_1/B_0) and angle of internal friction of bottom layer are increased while keeping rest of the parameter as constant. From the comparison, in Tables 11 and 12, it is seen that the present analysis gives relatively closer value with Eshkevari et al. (2019).

8.1 Numerical Example

In this section, a numerical example for the case of weak over strong clay soil is discussed using Eq. (62). The results are compared with the results of available solutions. The numerical solution determines the ultimate bearing capacity of strip footing of 4 m width, positioned on top of a two-layered clayey soil. The soil profile consists of a 2-m deep top layer with an undrained shear strength of 20 kPa and stronger bottom layer with an undrained shear strength of 25 kPa; the angle of internal friction is zero for both layers in the undrained loading condition. The ultimate bearing capacity obtained from the present study is approximately 107 kPa. Ahmadi and Kouchaki (2016) have calculated an ultimate bearing capacity of 105 kPa for this problem, which is (− 1.86%) lower than the present study. Meyerhof and Hanna (1975) calculated an ultimate bearing capacity of 110 kPa (+ 2.803%), which is higher than the present result. Merifield et al. (1999) and Michalowski (2002) have calculated an upper bound of 109.2 kPa (+ 2.06%), which is higher than the present result. Chen (1975) has calculated upper bound value of 115 kPa (+ 7.67%), which is even higher than upper-bound value of Merifield et al. (1999) and Michalowski (2002). Zhu (2004) has evaluated the ultimate bearing capacity of 108.4 kPa (+ 1.30%), whereas Merifield et al. (1999) have calculated a lower-bound value of 100 kPa (− 6.54), which is lower than Ahmadi and Kouchaki (2016). From this numerical example, it is seen that the present study gives values closure to Ahmadi and Kouchaki (2016), Zhu (2004), upper-bound solution of Merifield et al. (1999).

9 Conclusions

The bearing capacity of strip footing resting on two-layered $c-\phi$ soil has been analytically determined by using a new pseudo-dynamic limit equilibrium approach in conjunction with particle swarm optimization. Simultaneous resistance of unit weight, surcharge and cohesion is taken into account to evaluate the new pseudo-dynamic bearing capacity coefficients in which linear failure surface is considered. On the basis of analysis, it is seen that keeping the bottom layer's value constant, when we increase the corresponding values of upper layer like γ, c, ϕ, then the values of seismic bearing capacity increase or vice versa. Seismic bearing capacity value decreases if we increase the value of horizontal and vertical seismic acceleration coefficients. The analytical results are presented in terms of single bearing capacity coefficients ($N_{\gamma''}$). Results as obtained from the present analysis are well comparable with earlier experimental, numerical and analytical solutions. So, the results obtained from the present analysis as given in tabular form can be used to evaluate the bearing capacity of foundation resting on two-layered soil under seismic loading condition. Further research work can be done for the problem using a new pseudo-dynamic method considering logarithmic failure surface.

Appendix 1

$$c_{s_1 z_1} = \cos k_{s_1 z_1} \cosh k_{s_2 z_2} = \cos\left(\frac{y_{s_1} z_1}{h_1}\right) \cosh\left(\frac{y_{s_2} z_2}{h_2}\right) \quad c_{s_1} = \cos y_{s_1} \cosh y_{s_2}$$

$$s_{s_1 z_1} = -\sin k_{s_1 z_1} \sinh k_{s_2 z_2} = \sin\left(\frac{y_{s_1} z_1}{h_1}\right) \sinh\left(\frac{y_{s_2} z_2}{h_2}\right) \quad s_{s_1} = -\sin y_{s_1} \sinh y_{s_2}$$

$$I_{s_3} = \int_0^{h_2} c_{s_2 z_2}(h_2 - z_2)\mathrm{d}z_2 = -\frac{h_2^2}{\left(y_{s_3}^2 + y_{s_4}^2\right)^2}\left[2y_{s_3} y_{s_4} \sin y_{s_3} \sinh y_{s_4} + \left(y_{s_3}^2 - y_{s_4}^2\right) - \left(y_{s_3}^2 - y_{s_4}^2\right) \cos y_{s_3} \cosh y_{s_4}\right]$$

$$I_{s_1} = \int_0^{h_1} c_{s_1 z_1}(B_0 \tan\alpha_{A_1} - z_1)\mathrm{d}z_1 = -\frac{h_1^2}{\left(y_{s_1}^2 + y_{s_2}^2\right)}\left[\begin{array}{r} -y_{s_1}^2 + y_{s_2}^2 + \cosh(y_{s_2})\left\{(y_{s_1}^2 - y_{s_2}^2)\cos y_{s_1} + y_{s_1}(y_{s_1}^2 + y_{s_2}^2)\sin y_{s_1}\right\} + y_{s_2} \\ \left\{(y_{s_1}^2 + y_{s_2}^2)\cos y_{s_1} - 2y_{s_1}\sin y_{s_1}\right\}\sinh(y_{s_2}) \end{array}\right] + \frac{B_0 h_1 \tan\alpha_{A_1}\left\{y_{s_1}\cosh y_{s_2}\sin y_{s_1} + y_{s_2}\cos y_{s_1}\sinh y_{s_2}\right\}}{(y_{s_1}^2 + y_{s_2}^2)}$$

$$I_{s_2} = \int_0^{h_1} s_{s_1 z_1}(B_0 \tan\alpha_{A_1} - z_1)\mathrm{d}z_1 = \frac{h_1^2}{\left(y_{s_1}^2 + y_{s_2}^2\right)}\left[\begin{array}{r} -2y_{s_1} y_{s_2} + y_{s_2}\cosh(y_{s_2})\left\{2y_{s_1}\cos y_{s_1} + (y_{s_1}^2 + y_{s_2}^2)\sin y_{s_1}\right\} - \\ \left\{y_{s_1}(y_{s_1}^2 + y_{s_2}^2)\cos y_{s_1} + (y_{s_1}^2 - y_{s_2}^2)\sin y_{s_1}\right\}\sinh(y_{s_2}) \end{array}\right] + \frac{B_0 h_1 \tan\alpha_{A_1}\left\{-y_{s_2}\cosh y_{s_2}\sin y_{s_1} + y_{s_1}\cos y_{s_1}\sinh y_{s_2}\right\}}{(y_{s_1}^2 + y_{s_2}^2)}$$

$$A_{h_1} = \frac{h_1^2}{\left(y_{s_1}^2 + y_{s_2}^2\right)}\left[\begin{array}{r} \left(y_{s_2}^2 - y_{s_1}^2\right)\left(\cos^2 y_{s_1} + \sinh^2 y_{s_2}\right) - y_{s_1}\left(y_{s_1}^2 + y_{s_2}^2\right)\sin y_{s_1}\cos y_{s_1} \\ -y_{s_2}\left(y_{s_1}^2 + y_{s_2}^2\right)\sinh y_{s_2}\cosh y_{s_2} + 2y_{s_1} y_{s_2}\sin y_{s_1}\sinh y_{s_2} - \left(y_{s_2}^2 - y_{s_1}^2\right)\cos y_{s_1}\cosh y_{s_2} \end{array}\right] + \frac{B_0 h_1 \tan\alpha_{A_1}(y_{s_1}\sin y_{s_1}\cos y_{s_1} + y_{s_2}\cosh y_{s_2}\sinh y_{s_2}}{\left(y_{s_1}^2 + y_{s_2}^2\right)}$$

$$B_{h_1} = \frac{h_1^2}{(y_{s_1}^2 + y_{s_2}^2)}\left[\begin{array}{r} y_{s_1}(y_{s_1}^2 + y_{s_2}^2)\sinh y_{s_2}\cosh y_{s_2} - y_{s_2}(y_{s_1}^2 + y_{s_2}^2)\sin y_{s_1}\cos y_{s_1} - 2y_{s_1} y_{s_2}\left(\cos^2 y_{s_1} + \sinh^2 y_{s_2}\right) \\ +2y_{s_1} y_{s_2}\cos y_{s_1}\cosh y_{s_2} + (y_{s_2}^2 - y_{s_1}^2)\sin y_{s_1}\sinh y_{s_2} \end{array}\right] + \frac{B_0 h_1 \tan\alpha_{A_1}(y_{s_2}\sin y_{s_1}\cos y_{s_1} - y_{s_1}\cosh y_{s_2}\sinh y_{s_2})}{(y_{s_1}^2 + y_{s_2}^2)}$$

$$I_{s_4} = \int_0^{h_2} s_{s_2 z_2}(h_2 - z_2)\mathrm{d}z_2$$
$$= \frac{h_2^2}{\left(y_{s_3}^2 + y_{s_4}^2\right)^2}\left[\left(y_{s_3}^2 - y_{s_4}^2\right)\sin y_{s_3}\sinh y_{s_4} + 2y_{s_3}y_{s_4}\cos y_{s_3}\cosh y_{s_4} - 2y_{s_3}y_{s_4}\right]$$

$$A_{h_2} = \frac{2y_{s_3}y_{s_4}\sin y_{s_3}\sinh y_{s_4} + \left(y_{s_3}^2 - y_{s_4}^2\right)(\cos y_{s_3}\cosh y_{s_4} - \cos^2 y_{s_3} - \sinh^2 y_{s_4})}{(\cos^2 y_{s_3} + \sinh^2 y_{s_4})\left(y_{s_3}^2 + y_{s_4}^2\right)^2}$$

$$B_{h_2} = \frac{2y_{s_3}y_{s_4}(\cos y_{s_3}\cosh y_{s_4} - \cos^2 y_{s_3} - \sinh^2 y_{s_4}) - \left(y_{s_3}^2 - y_{s_4}^2\right)\sin y_{s_3}\sinh y_{s_4}}{\left(\cos^2 y_{s_3} + \sinh^2 y_{s_4}\right)\left(y_{s_3}^2 + y_{s_4}^2\right)^2}$$

Appendix 2

$$I_{s_5} = \int_0^{h_1} c_{s_3 z_1}(B_0\tan\alpha_{A_1} - z_1)\mathrm{d}z_1$$
$$= \frac{h_1^2\left(y_{s_5}^2 - y_{s_6}^2\right)\tan\alpha_{p_2}}{\left(y_{s_5}^2 + y_{s_6}^2\right)^2} + \frac{y_{s_5}\cosh y_{s_6}\sin y_{s_5} + y_{s_6}\sinh y_{s_6}\cos y_{s_5}}{\left(y_{s_5}^2 + y_{s_6}^2\right)}(h_1h_2\tan\alpha_{p_1} + h_1^2\tan\alpha_{p_2})$$
$$- \frac{h_1^2\left(y_{s_5}^2 + y_{s_6}^2\right)(y_{s_6}\cos y_{s_5}\sinh y_{s_6} + y_{s_5}\cosh y_{s_6}\sin y_{s_5})\tan\alpha_{p_2}}{\left(y_{s_5}^2 + y_{s_6}^2\right)^2} + \frac{y_{s_6}2h_1^2y_{s_5}\sin y_{s_5}\sinh y_{s_6} - h_1^2\cosh y_{s_6}\left(y_{s_5}^2 - y_{s_6}^2\right)\cos y_{s_5}}{\left(y_{s_5}^2 + y_{s_6}^2\right)^2}$$

$$I_{s_6} = \int_0^{h_1} c_{s_3 z_1}(B_0\tan\alpha_{A_1} - z_1)\mathrm{d}z_1$$
$$= \frac{h_1^2\left(y_{s_5}^2 + y_{s_6}^2\right)(y_{s_6}\cosh y_{s_6}\sin y_{s_5} - y_{s_5}\cos y_{s_5}\sinh y_{s_6})\tan\alpha_{p_2}}{\left(y_{s_5}^2 + y_{s_6}^2\right)^2} - \frac{2h_1^2y_{s_5}y_{s_6}\tan\alpha_{p_2}}{\left(y_{s_5}^2 + y_{s_6}^2\right)^2}$$
$$+ \frac{h_1^2\left\{2y_{s_5}y_{s_6}\cos y_{s_5}\cosh y_{s_6} - \left(y_{s_6}^2 - y_{s_5}^2\right)\sin y_{s_5}\sinh y_{s_6}\right\}\tan\alpha_{p_2}}{\left(y_{s_5}^2 + y_{s_6}^2\right)^2}$$
$$- \frac{(y_{s_6}\cosh y_{s_6}\sin y_{s_5} - y_{s_5}\sinh y_{s_6}\cos y_{s_5})}{\left(y_{s_5}^2 + y_{s_6}^2\right)}\left(h_1h_2\tan\alpha_{p_1} + h_1^2\tan\alpha_{p_2}\right)$$

$$B_{\mathrm{h}_3} = -\frac{\mathrm{h}_1^2 \tan\alpha_{p_2}}{\left(y_{\mathrm{s}_5}^2 + y_{\mathrm{s}_6}^2\right)^2}\left[\cos y_{\mathrm{s}_5}\cosh y_{\mathrm{s}_6}\left(y_{\mathrm{s}_5}^2 - y_{\mathrm{s}_6}^2\right)\sin y_{\mathrm{s}_5}\sinh y_{\mathrm{s}_6} + 2y_{\mathrm{s}_5}y_{\mathrm{s}_6}\cos y_{\mathrm{s}_5}\right]$$
$$+ \frac{[y_{\mathrm{s}_5}\sinh y_{\mathrm{s}_6}\cosh y_{\mathrm{s}_6} - y_{\mathrm{s}_6}\sin y_{\mathrm{s}_5}\cos y_{\mathrm{s}_5}(\cosh^2 y_{\mathrm{s}_6} + \sinh^2 y_{\mathrm{s}_6})]}{\left(y_{\mathrm{s}_5}^2 + y_{\mathrm{s}_6}^2\right)}(h_1 h_2 \tan\alpha_{p_1} + h_1^2 \tan\alpha_{p_2})$$
$$+ \frac{\mathrm{h}_1^2}{\left(y_{\mathrm{s}_5}^2 + y_{\mathrm{s}_6}^2\right)}[y_{\mathrm{s}_6}\sin y_{\mathrm{s}_5}\cos y_{\mathrm{s}_5}(\cosh^2 y_{\mathrm{s}_6} + \sinh^2 y_{\mathrm{s}_6}) - y_{\mathrm{s}_5}\cosh y_{\mathrm{s}_6}\sinh y_{\mathrm{s}_6}\cos 2y_{\mathrm{s}_5}]\tan\alpha_{p_2}$$
$$+ \frac{\mathrm{h}_1^2 \tan\alpha_{p_2}}{\left(y_{\mathrm{s}_5}^2 + y_{\mathrm{s}_6}^2\right)^2}\left[2y_{\mathrm{s}_5}y_{\mathrm{s}_6}\left\{\cos^2 y_{\mathrm{s}_6} - \sinh^2 y_{\mathrm{s}_5}(\cosh^2 y_{\mathrm{s}_6} + \sinh^2 y_{\mathrm{s}_6})\right\}\right]$$

$$I_{\mathrm{s}_7} = \int_0^{\mathrm{h}_2} c_{\mathrm{s}_4 z_2}(h_2 - z_2)\mathrm{d}z_2$$
$$= -\frac{\mathrm{h}_2^2}{\left(y_{\mathrm{s}_7}^2 + y_{\mathrm{s}_8}^2\right)^2}\left[2y_{\mathrm{s}_7}y_{\mathrm{s}_8}\sin y_{\mathrm{s}_7}\sinh y_{\mathrm{s}_8} + \left(y_{\mathrm{s}_7}^2 - y_{\mathrm{s}_8}^2\right) - \left(y_{\mathrm{s}_7}^2 - y_{\mathrm{s}_8}^2\right)\cos y_{\mathrm{s}_7}\cosh y_{\mathrm{s}_8}\right]$$

$$I_{\mathrm{s}_4} = \int_0^{\mathrm{h}_2} \mathrm{s}_{\mathrm{s}_4 z_2}(h_2 - z_2)\mathrm{d}z_2$$
$$= \frac{\mathrm{h}_2^2}{\left(y_{\mathrm{s}_7}^2 + y_{\mathrm{s}_8}^2\right)^2}\left[\left(y_{\mathrm{s}_7}^2 - y_{\mathrm{s}_8}^2\right)\sin y_{\mathrm{s}_7}\sinh y_{\mathrm{s}_8} + 2y_{\mathrm{s}_7}y_{\mathrm{s}_8}\cos y_{\mathrm{s}_7}\cosh y_{\mathrm{s}_8} - 2y_{\mathrm{s}_7}y_{\mathrm{s}_8}\right]$$

$$A_{\mathrm{h}_4} = \frac{2y_{\mathrm{s}_7}y_{\mathrm{s}_8}\sin y_{\mathrm{s}_7}\sinh y_{\mathrm{s}_8} + \left(y_{\mathrm{s}_7}^2 - y_{\mathrm{s}_8}^2\right)\left(\cos y_{\mathrm{s}_7}\cosh y_{\mathrm{s}_8} - \cos^2 y_{\mathrm{s}_7} - \sinh^2 y_{\mathrm{s}_8}\right)}{\left(\cos^2 y_{\mathrm{s}_7} + \sinh^2 y_{\mathrm{s}_8}\right)\left(y_{\mathrm{s}_7}^2 + y_{\mathrm{s}_8}^2\right)^2}$$

$$B_{\mathrm{h}_4} = \frac{2y_{\mathrm{s}_7}y_{\mathrm{s}_8}\left(\cos y_{\mathrm{s}_7}\cosh y_{\mathrm{s}_8} - \cos^2 y_{\mathrm{s}_7} - \sinh^2 y_{\mathrm{s}_8}\cos y_{\mathrm{s}_7}\cosh y_{\mathrm{s}_8} - \cos^2 y_{\mathrm{s}_7} - \sinh^2 y_{\mathrm{s}_8}\right) - \left(y_{\mathrm{s}_7}^2 - y_{\mathrm{s}_8}^2\right)\sin y_{\mathrm{s}_7}\sinh y_{\mathrm{s}_8}}{\left(\cos^2 y_{\mathrm{s}_7} + \sinh^2 y_{\mathrm{s}_8}\right)\left(y_{\mathrm{s}_7}^2 + y_{\mathrm{s}_8}^2\right)^2}$$

Appendix 3

$$a_1 = \left(\frac{\mathrm{h}_1}{B_0}\cot\alpha_{p1} + 2\frac{\mathrm{h}_2}{B_0}\cot\alpha_{\mathrm{p2}}\right)\frac{\mathrm{h}_1}{B_0}\frac{\gamma_1}{\bar{\gamma}}\left\{\frac{\sin\left(\phi_1+\alpha_{p1}\right)}{\cos\left(\phi_1+\alpha_{p1}+\delta_1\right)}\right\} - 2\frac{\gamma_1}{\bar{\gamma}}\frac{\mathrm{h}_1}{B_0}\frac{\mathrm{h}_2}{B_0}\cot\alpha_{\mathrm{p2}}$$
$$\left\{\frac{\left\{1 \pm a_{\mathrm{i_v}}(h_2,t)/g\right\}\sin\left(\phi_1+\alpha_{\mathrm{p1}}\right) + \left\{a_{\mathrm{i_h}}(h_2,t)/g\right\}\tan\phi_2\cos\left(\phi_1+\alpha_{p1}\right)}{\cos\left(\phi_1+\alpha_{p1}+\delta_1\right)}\right\} + \left(\frac{\mathrm{h}_2}{B_0}\right)^2\cot\alpha_{\mathrm{p2}}\frac{\gamma_2}{\bar{\gamma}}\left\{\frac{\sin\left(\phi_2+\alpha_{\mathrm{p2}}\right)}{\cos\left(\phi_2+\alpha_{\mathrm{p2}}+\delta_2\right)}\right\}$$
$$+ 2\frac{\gamma_1}{\bar{\gamma}}\frac{\mathrm{h}_1}{B_0}\frac{\mathrm{h}_2}{B_0}\cot\alpha_{\mathrm{p2}}\left\{\frac{1 \pm a_{\mathrm{t_v}}(h_1,t)/g\sin\left(\phi_2+\alpha_{\mathrm{p2}}\right) + a_{\mathrm{t_h}}(h_1,t)/g\tan\phi_1\cos\left(\phi_2+\alpha_{\mathrm{p2}}\right)}{\cos\left(\phi_2+\alpha_{\mathrm{p2}}+\delta_2\right)}\right\} - \left(2 - \frac{\mathrm{h}_1}{B_0}\cot\alpha_{\mathrm{A1}}\right)\frac{\mathrm{h}_1}{B_0}\frac{\gamma_1}{\bar{\gamma}}$$
$$\left\{\frac{\sin\left(\alpha_{\mathrm{A1}}-\phi_1\right)}{\cos\left(\alpha_{\mathrm{A1}}-\phi_1-\delta_1\right)}\right\} + 2\frac{\gamma_1}{\bar{\gamma}}\frac{\mathrm{h}_1}{B_0}\left(1 - \frac{\mathrm{h}_1}{B_0}\cot\alpha_{\mathrm{A1}}\right)\left\{\frac{1 \pm a_{\mathrm{i_v}}(h_2,t)/g\sin\left(\alpha_{\mathrm{A1}}-\phi_1\right) + a_{\mathrm{i_h}}(h_2,t)/g\tan\phi_2\cos\left(\alpha_{\mathrm{A1}}-\phi_1\right)}{\cos\left(\alpha_{\mathrm{A1}}-\phi_1-\delta_1\right)}\right\}$$
$$- \left(1 - \frac{\mathrm{h}_1}{B_0}\cot\alpha_{\mathrm{A1}}\right)\frac{\mathrm{h}_2}{B_0}\frac{\gamma_2}{\bar{\gamma}}\left\{\frac{\sin\left(\alpha_{\mathrm{A2}}-\phi_2\right)}{\cos\left(\alpha_{\mathrm{A2}}-\phi_2-\delta_2\right)}\right\}$$
$$- 2\frac{\gamma_1}{\bar{\gamma}}\frac{\mathrm{h}_1}{B_0}\left(1 - \frac{\mathrm{h}_1}{B_0}\cot\alpha_{\mathrm{A1}}\right)\left\{\frac{\left\{1 \pm a_{\mathrm{t_v}}(h_1,t)/g\right\}\sin\left(\alpha_{\mathrm{A2}}-\phi_2\right) + a_{\mathrm{t}}h(h_1,t)/g\tan\phi_1\cos\left(\alpha_{\mathrm{A2}}-\phi_2\right)}{\cos\left(\alpha_{\mathrm{A2}}-\phi_2-\delta_2\right)}\right\}$$
$$- 2\frac{Q_{\mathrm{t_{h(BJKD)}}}}{\bar{\gamma}B_0^2}\frac{\cos\left(\phi_1+\alpha_{p1}\right)}{\cos\left(\phi_1+\alpha_{p1}+\delta_1\right)} + 2\frac{Q_{t_{v(BJKD)}}}{\bar{\gamma}B_0^2}\frac{\sin\left(\phi_1+\alpha_{p1}\right)}{\cos\left(\phi_1+\alpha_{p1}+\delta_1\right)} - 2\frac{(Q_{\mathrm{h_{(DKF)}}})_{\mathrm{R}}}{\bar{\gamma}B_0^2}\frac{\cos\left(\phi_2+\alpha_{\mathrm{p2}}\right)}{\cos\left(\phi_2+\alpha_{\mathrm{p2}}+\delta_2\right)} + 2\frac{(Q_{v_{(\mathrm{DKF})}})_{\mathrm{R}}}{\bar{\gamma}B_0^2}\frac{\sin\left(\phi_2+\alpha_{\mathrm{p2}}\right)}{\cos\left(\phi_2+\alpha_{\mathrm{p2}}+\delta_2\right)}$$
$$- 2\frac{Q_{\mathrm{t_{h(ABDE)}}}}{\bar{\gamma}B_0^2}\frac{\cos\left(\alpha_{\mathrm{A1}}-\phi_1\right)}{\cos\left(\alpha_{\mathrm{A1}}-\phi_1-\delta_1\right)} - 2\frac{(Q_{\mathrm{h_{(EDF)}}})_{\mathrm{R}}}{\bar{\gamma}B_0^2}\frac{\cos\left(\alpha_{\mathrm{A2}}-\phi_2\right)}{\cos\left(\alpha_{\mathrm{A2}}-\phi_2-\delta_2\right)} + 2\frac{Q_{t_{v(ABDE)}}}{\bar{\gamma}B_0^2}\frac{\sin\left(\alpha_{\mathrm{A1}}-\phi_1\right)}{\cos\left(\alpha_{\mathrm{A1}}-\phi_1-\delta_1\right)}$$
$$+ 2\frac{(Q_{v_{(\mathrm{EDF})}})_{\mathrm{R}}}{\bar{\gamma}B_0^2}\frac{\sin\left(\alpha_{\mathrm{A2}}-\phi_2\right)}{\cos\left(\alpha_{\mathrm{A2}}-\phi_2-\delta_2\right)}$$

$$d_1 = 2\frac{c_2}{\bar{c}}\frac{\mathrm{h}_2}{B_0}\frac{\sin\left(\phi_2+\alpha_{\mathrm{p2}}\right)}{\cos\left(\phi_2+\alpha_{\mathrm{p2}}+\delta_2\right)} + \frac{c_1}{\bar{c}}\frac{\mathrm{h}_2}{B_0}\cot\alpha_{\mathrm{p2}}\frac{\cos\left(\phi_2+\alpha_{\mathrm{p2}}\right)}{\cos\left(\phi_2+\alpha_{\mathrm{p2}}+\delta_2\right)} + \frac{c_2}{\bar{c}}\frac{\mathrm{h}_2}{B_0}\cot\alpha_{\mathrm{p2}}\frac{\cos\left(\phi_2+\alpha_{\mathrm{p2}}\right)}{\cos\left(\phi_2+\alpha_{\mathrm{p2}}+\delta_2\right)}$$

$$d_1 = 2\frac{c_2}{\bar{c}}\frac{\mathrm{h}_2}{B_0}\frac{\sin\left(\phi_2+\alpha_{\mathrm{p2}}\right)}{\cos\left(\phi_2+\alpha_{\mathrm{p2}}+\delta_2\right)} + \frac{c_1}{\bar{c}}\frac{\mathrm{h}_2}{B_0}\cot\alpha_{\mathrm{p2}}\frac{\cos\left(\phi_2+\alpha_{\mathrm{p2}}\right)}{\cos\left(\phi_2+\alpha_{\mathrm{p2}}+\delta_2\right)} + \frac{c_2}{\bar{c}}\frac{\mathrm{h}_2}{B_0}\cot\alpha_{\mathrm{p2}}\frac{\cos\left(\phi_2+\alpha_{\mathrm{p2}}\right)}{\cos\left(\phi_2+\alpha_{\mathrm{p2}}+\delta_2\right)}$$
$$+ 2\frac{c_1}{\bar{c}}\frac{\mathrm{h}_1}{B_0}\frac{\sin\left(\phi_1+\alpha_{p1}\right)}{\cos\left(\phi_1+\alpha_{p1}+\delta_1\right)} + \frac{c_1}{\bar{c}}\frac{\mathrm{h}_1}{B_0}\cot\alpha_{p1}\frac{\cos\left(\phi_1+\alpha_{p1}\right)}{\cos\left(\phi_1+\alpha_{p1}+\delta_1\right)} - \frac{c_1}{\bar{c}}\frac{\mathrm{h}_2}{B_0}\cot\alpha_{\mathrm{p2}}\frac{\cos\left(\phi_1+\alpha_{p1}\right)}{\cos\left(\phi_1+\alpha_{p1}+\delta_1\right)}$$
$$+ 2\frac{c_1}{\bar{c}}\frac{\mathrm{h}_1}{B_0}\frac{\sin\left(\alpha_{\mathrm{A1}}-\phi_1\right)}{\cos\left(\alpha_{\mathrm{A1}}-\phi_1-\delta_1\right)} + \frac{c_1}{\bar{c}}\frac{\cos\left(\alpha_{\mathrm{A1}}-\phi_1\right)}{\cos\left(\alpha_{\mathrm{A1}}-\phi_1-\delta_1\right)} + 2\frac{c_2}{\bar{c}}\frac{\mathrm{h}_2}{B_0}\frac{\sin\left(\alpha_{\mathrm{A2}}-\phi_2\right)}{\cos\left(\alpha_{\mathrm{A2}}-\phi_2-\delta_2\right)}$$
$$+ \frac{c_2}{\bar{c}}\frac{\mathrm{h}_2}{B_0}\cot\alpha_{\mathrm{A2}}\frac{\cos\left(\alpha_{\mathrm{A1}}-\phi_1\right)}{\cos\left(\alpha_{\mathrm{A1}}-\phi_1-\delta_1\right)} - \frac{c_1}{\bar{c}}\frac{\cos\left(\alpha_{\mathrm{A2}}-\phi_2\right)}{\cos\left(\alpha_{\mathrm{A2}}-\phi_2-\delta_2\right)} + \frac{c_1}{\bar{c}}\frac{\mathrm{h}_1}{B_0}\cot\alpha_{\mathrm{A1}}\frac{\cos\left(\alpha_{\mathrm{A2}}-\phi_2\right)}{\cos\left(\alpha_{\mathrm{A2}}-\phi_2-\delta_2\right)}$$

$$b_1 = 2\frac{\gamma_1}{\bar{\gamma}}\frac{D_f}{B_0}\left(\frac{h_1}{B_0}\cot\alpha_{p1}+\frac{h_2}{B_0}\cot\alpha_{p2}\right)\left\{\frac{(1\pm k_v)\sin(\phi_1+\alpha_{p1})-k_h\cos(\phi_1+\alpha_{p1})}{\cos(\phi_1+\alpha_{p1}+\delta_1)}\right\}$$
$$-\left\{\frac{2\frac{\gamma_1}{\bar{\gamma}}\frac{D_f}{B_0}\left(\frac{h_1}{B_0}\cot\alpha_{p1}+\frac{h_2}{B_0}\cot\alpha_{p2}\right)}{\left(\frac{h_1}{B_0}+\frac{h_1}{B_0}\cot\alpha_{p1}+\frac{h_2}{B_0}\cot\alpha_{p2}\right)}\right\}\frac{h_2}{B_0}\cot\alpha_{p2}\left\{\frac{1\pm a_{i_v}(h_2,t)/g\sin(\phi_1+\alpha_{p1})+a_{i_h}(h_2,t)/g\tan\phi_2\cos(\phi_1+\alpha_{p1})}{\cos(\phi_1+\alpha_{p1}+\delta_1)}\right\}$$
$$+2\frac{\gamma_1}{\bar{\gamma}}\frac{D_f}{B_0}\frac{\left(\frac{h_1}{B_0}\cot\alpha_{p1}+\frac{h_2}{B_0}\cot\alpha_{p2}\right)}{\left(\frac{h_1}{B_0}+\frac{h_1}{B_0}\cot\alpha_{p1}+\frac{h_2}{B_0}\cot\alpha_{p2}\right)}\frac{h_2}{B_0}\cot\alpha_{p2}\left\{\frac{1\pm a_{t_v}(h_1,t)/g\sin(\phi_2+\alpha_{p2})+a_{t_h}(h_1,t)/g\tan\phi_1\cos(\phi_2+\alpha_{p2})}{\cos(\phi_2+\alpha_{p2}+\delta_2)}\right\}$$

$$e_1 = \left\{\frac{\{(1\pm k_v)\}\sin(\alpha_{A1}-\phi_1)+k_h\cos(\alpha_{A1}-\phi_1)}{\cos(\alpha_{A1}-\phi_1-\delta_1)}\right\}-\left\{\frac{\left(1-\frac{h_1}{B_0}\cot\alpha_{A1}\right)}{1+\frac{h_1}{B_0}}\right\}$$
$$\left\{\frac{\left(1\pm a_{i_v}(h_2,t)/g\right)\sin(\alpha_{A1}-\phi_1)+\left\{a_{i_h}(h_2,t)/g\right\}\tan\phi_2\cos(\alpha_{A1}-\phi_1)}{\cos(\alpha_{A1}-\phi_1-\delta_1)}\right\}+\left\{\frac{\left(1-\frac{h_1}{B_0}\cot\alpha_{A1}\right)}{1+\frac{h_1}{B_0}}\right\}$$
$$\left\{\frac{\left(1\pm a_{t_v}(h_1,t)/g\right)\sin(\alpha_{A2}-\phi_2)+\left\{a_{t_h}(h_1,t)/g\right\}\tan\phi_1\cos(\alpha_{A2}-\phi_2)}{\cos(\alpha_{A2}-\phi_2-\delta_2)}\right\}$$

References

Ahmadi MM, Kouchaki B (2016) New and simple equations for ultimate bearing capacity of strip footings on Two layered clays: numerical study. Int J Geomech. https://doi.org/10.1061/(ASCE)GM.1943-5622.0000615

Bellezza I (2014) A new pseudo-dynamic approach for seismic active soil thrust. Geotech Geol Eng 32(2):561–576

Bellezza I (2015) Seismic active soil thrust on walls using a new pseudo-dynamic approach. Geotech Geol Eng 33(4):795–812

Benmebarek S, Benmoussa S, Belounar L, Benmebarek N (2012) Bearing capacity of shallow foundation on two clay layers by numerical approach. Geotech Geological Eng. https://doi.org/10.1007/s10706-012-9513-6

Bera KM, Sasmal S (2017) Ultimate bearing capacity analysis of square footing on two-layered soil. J Geotech Stud Mater J 2(1):1–11

Biswas N, Ghosh P (2017) Bearing capacity factors for isolated surface strip footing resting on multi-layered reinforced soil bed. Indian Geotech J. https://doi.org/10.1007/s40098-017-0293-z

Bowles JE (1996) Foundation analysis and design, 5th edn. McGraw-Hill, New York

Budhu M, Al-Karni A (1993) Seismic bearing capacity of soils. Geotechnique 93(1):181–187. https://doi.org/10.1680/geot.1993.43.1.181

Button, SJ (1953) The bearing capacity of footing on two-layer cohesive sub-soil. In: Proceedings of the 3rd international conference on soil mechanics and foundation engineering,vol 1, pp 332–335

Chen WF (1975) Limit analysis and soil plasticity. Elsevier, Amsterdam

Cheng YM, Li L, Chi SC (2007) Performance studies on six heuristic global optimization methods in the location ofcritical slip surface. Comput Geotech 34(6):462–484. https://doi.org/10.1016/j.compgeo.2007.01.004

Choudhury D, Nimbalkar S (2005) Seismic passive resistance by pseudo-dynamic method. Geotechnique 55(9):699–702

Choudhury D, Subba Rao KS (2005) Seismic uplift capacity of inclined strip anchors. Can Geotech J 42(1):263–271. https://doi.org/10.1139/t09-074

Choudhury D, Subba Rao KS (2006) Seismic bearing capacity of shallow strip footings embedded in slope. Int J Geomech 6(3):176. https://doi.org/10.1061/(asce)1532-3641

Debnath L, Ghosh S (2018) Pseudo-static analysis of shallow strip footing resting on two-layered soil. Int J Geomech 107(7):915–927. https://doi.org/10.1061/(ASCE)GM.1943-5622.0001049

Drominex L, Pecker A (1995) Seismic bearing capacity of foundation on cohesionless soils. J Geotech Eng ASCE 121(3):300–303

Engelbrecht AP (2007) Computational intelligence: an introduction. Wiley, London

Eshkevari SS, Abbo JA, Kouretzis G (2019) Bearing capacity of strip footings on Layered sands. Comput Geotech. https://doi.org/10.1016/j.compgeo.2019.103101

Eurocode7(1996) Calcul Geotechnique. AFNOR, XP, ENV 1997-1 (see Sieffert and Bay- Gress, 2000)

Farah CA (2004) Ultimate bearing capacity of shallow foundations on layered soils. M.Sc. thesis Civil and Environmental Engineering Concordia Univ., Quebec

Florkiewicz A (1989) Upper bound to bearing capacity of layered soils. Can Geotech J. https://doi.org/10.1139/t89-084

Ghazavi M, Eghbali AH (2008) A simple limit equilibrium approach for calculation of ultimate bearing capacity of shallow foundations on two-layered granular soils. Geotech Geological Eng 26(5):535–542. https://doi.org/10.1007/s10706-008-9187-2

Ghosh P (2008) Upper bound solutions of bearing capacity of strip footing by pseudo-dynamic approach. Acta Geotech. https://doi.org/10.1007/s11440-008-0058-z

Ghosh S, Debnath L (2017) Seismic bearing capacity of shallow strip footing with coulomb failure mechanism using limit equilibrium method. Geotech Geological Eng. https://doi.org/10.1007/s10706-017-0268-y

Griffiths DV (1982) Computation of bearing capacity factors using finite elements. Geotechnique 32(3):195–202

Haghbin M (2016) Bearing capacity of strip footings resting on granular soil overlaying soft clay. Int J Civ Eng. https://doi.org/10.1007/s40999-016-0067-5
Hanna AM (1981) Foundations on strong sand overlying weak sand. J Geotech Geoenviron Eng 102(7):915–927
Hanna AM (1982) Bearing capacity of foundations on a weak sand layer overlying a strong deposit. Can Geotech Eng 19:392–396
Hanna AM, Meyerhof GG (1979) Ultimate bearing capacity of foundations on a three layered soils. Can Geotech J 16:412–414
Hansen JB (1970) A revised and extended formula for bearing capacity. Geotek Inst Bull 28:5–11
Hossain MS, El-Shafie A (2014) Evolutionary techniques versus swarm intelligences: application in reservoir release optimization. Neural Comput Appl 24(7):1583–1594. https://doi.org/10.1007/s00521-013-1389-8
Jadar MC, Ghosh S (2017) Seismic bearing capacity of shallow strip footing using horizontal slice method. Int J Geotech Engg 11(1):38–50
Jahani M, Oulapour M, Haghighi A (2018) Evaluation of the seismic bearing capacity of shallow foundations located on the two-layered clayey soils. Iran J Sci Technol Trans Civ Eng. https://doi.org/10.1007/s40996-018-0122-3
Kalatehjari R (2013) An improvised three-dimensional slope stability analysis based on limit equilibrium method by using particle swarm optimization. Dissertation, Universiti Teknologi Malaysia
Karamitros DK, Bouckovalas GD, Chaloulos YK, Andrianopoulos KI (2013) Numerical analysis of liquefaction-induced bearing capacity degradation of shallow foundations on a two-layered soil profile. Soil Dyn Earthq Eng 44:90–101
Kennedy J, Eberhart R (1995) Particle swarm optimization. In: Proceedings of IEEE international conference on neural networks, vol 4, pp 1942–1948
Khatri NV, Kumar J, Akhtar S (2017) Bearing capacity of foundations with inclusion of dense sand layer over loose sand strata. Int J Geomech. https://doi.org/10.1061/(asce)gm.1943-5622.0000980.06017018-1
Kumar A, Ohri ML, Bansal RK (2007) Bearing capacity tests of strip footings on reinforced layered soil. Geotech Geol Eng 25(2):139–150
Lotfizadeh RM, Kamalian M (2016) Estimating bearing capacity of strip footings over two-layered sandy soils using the characteristic lines method. Int J Civ Eng. https://doi.org/10.1007/s40999-016-0015-4
Merifield RS, Sloan SW, Yu HS (1999) Rigorous plasticity solutions for the bearing capacity of two-layered clays. Geotechnique 49(4):471–490
Meyerhof GG (1951) The ultimate bearing capacity of foundations. Geotechnique 2:301–332
Meyerhof GG, Hanna AM (1975) Ultimate bearing capacity of foundations on layered soils under inclined load. Can Geotech J 15(4):565–572
Michalowski RL (2002) Collapse load over two-layer clay foundation soils. Soils Found 42(1):1–7
Michalowski RL, Shi L (1995) Bearing capacity of footings over two layers foundation soils. J Geotech Eng. https://doi.org/10.1061/(ASCE)0733-9410(1995)121:5(421)
Pain A, Choudhury D, Bhattacharyya SK (2015) Seismic stability of retaining wall-soil sliding interaction using modified pseudo-dynamic method. Géotech Lett 5(1):56–61
Pain A, Choudhury D, Bhattacharyya SK (2017) Seismic passive earth resistance using modified pseudo-dynamic method. Earthq Eng Eng Vib 16:263–274
Prakash S, Saran S (1971) Bearing capacity of eccentrically loaded footings. J Soil Mech Found Div ASCE 97(1):95–117
Purushothamaraj P, Ramiaha K, Venkatakrishnrao NK (1974) Bearing capacity of strip footing on Two-Layered cohesion-Friction Soil. Can. Geotech Engg 11:32
Rajaei A, Keshavarz A, Ghahramaniz A (2018) Static and seismic bearing capacity of strip footings on sand overlying clay soils. Iran J Sci Technol Trans Civ Eng. https://doi.org/10.1007/s40996-018-0127-y
Reddy AS, Srinivasan RS (1967) Bearing capacity of footings on layered clays. J Soil Mech Found Div ASCE 93(2):83–99
Reynolds CW (1987) Flocks herds and schools: a distributed behavioral model. ACM SIGGRAPH Comput Gr 21(4):25–34
Richards R Jr, Elms DG, Budhu M (1993) Seismic bearing capacity and settlements of foundations. J Geotech Eng. https://doi.org/10.1061/(ASCE)0733-9410(1993)119
Saha A, Ghosh S (2015) Pseudo-dynamic bearing capacity of shallow strip footing resting on $c-\varphi$ soil considering composite failure surface. Int J Geotech Earthq Eng. https://doi.org/10.4018/ijgee.2015070102
Saha A, Ghosh S (2019) Modified pseudo-dynamic bearing capacity of shallow strip footing considering fully log-spiral passive zone with global centre. Iran J Sci Technol Trans Civ Eng. https://doi.org/10.1007/s40996-019-00271-1
Saran S (1971) Bearing capacity of footings under inclined loads. In: Seminar on foundation problems. Indian Geotechnical Society, New Delhi, 1971, vol 11, pp 4-5
Saran S, Agarwal RK (1991) Bearing capacity of eccentrically obliquely loaded footing. J Soil Mech Found Div ASCE 117(11):1669–1690
Saran S, Sud VK, Handa SC (1989) Bearing capacity of footings adjacent to slopes. J. Geotech Eng 115(4):553–573
Sharma LK, Singh TN (2017) Regression-based models for the prediction of unconfined compressive strength of artificially structured soil. In: Engineering with computers, pp 1–12
Singh R, Umrao RK, Ahmad M, Ansari MK, Sharma LK, Singh TN (2017) Prediction of geomechanical parameters using soft computing and multiple regression approach. Measurement 99:108–119
Sokolovski VV (1965) Statics of granular media. Pergam on Press, New York
Soubra AH (1994) Discussion of: seismic bearing capacity and settlement of foundations by R. Richards Jr, DG. Elms M. Budhu. Geotech Eng ASCE. https://doi.org/10.1061/(asce)0733-9410(1994)120:9(1634)
Soubra AH (1997) Seismic bearing capacity of shallow strip footings in seismic conditions. Proc Inst Civ Eng Geotech Eng 125(4):230–241
Soubra AH (1999) Upper bound solutions for bearing capacity of foundations. J Geotech Geoenviron Eng ASCE 125(1):59–69
Steedman RS, Zeng X (1990) The influence of phase on the calculation of pseudo-static earth pressure on a retaining wall. Geotechnique 40(1):103–112
Terzaghi K (1943) Theoretical soil mechanics. Wiley, New York
Vesic AS (1973) Analysis of ultimate loads of shallow foundations. J Soil Mech Found Div ASCE 99(1):45–73
Wang XC, Carter PJ (2002) Deep penetration of strip and circular footings into layered soil. Int J Geomech. https://doi.org/10.1061/(ASCE)1532-3641(2002)2:2(205)
Yuan C, Peng S, Zhang Z, Liu Z (2006) Seismic wave propagation in Kelvin–Voigt homogeneous visco-elastic media. Sci China, Ser D Earth Sci 49(2):147–153
Zhu M (2004) Bearing capacity of strip footings on two-layer clay soil by finite element method. In: Proceedings of ABAQUS, Inc., Boston, pp 777–787